CERN-TH/95-72
FTUAM-95/8

Fermionic Dispersion Relations in the Standard Model at Finite Temperature

C. Quimbay[1] **and S. Vargas-Castrillón**[2]

CERN, TH Division
CH-1211, Geneva 23
Switzerland

Abstract

We compute the one-loop dispersion relations at finite temperature for quarks, charged leptons and neutrinos in the Minimal Standard Model. The dispersion relations are calculated in two different plasma situations: for a vacuum expectation value v of the Higgs field $v \neq 0$ (broken electroweak symmetry) and for $v = 0$ (unbroken electroweak symmetry). The flavour and chiral non-degeneracy of the quasi-particle spectrum is studied. Numerical results show that the thermal effective masses for fermions in the broken phase have a smaller value than those in the unbroken phase. The temperature dependence of the top quark and electron neutrino thermal effective masses is also presented. Gauge invariance of one-loop dispersion relations is studied.

[1]On leave of absence from Dpto. de Física Teórica, Univ. Autónoma de Madrid, Cantoblanco, 28049 Madrid, and Centro Internacional de Física, Bogotá.

[2]On leave of absence from Dpto. de Física Teórica, Univ. Autónoma de Madrid, Cantoblanco, 28049 Madrid.

CERN-TH/95-72
April 1995

1 Introduction

The behaviour of the plasma in the high temperature regime plays a fundamental role in the attempts to explain several puzzles in cosmology, as for example the present baryon asymmetry of the universe [1, 2] in the electroweak scenario. When the temperature of the universe (T) was near the critical one of the cosmological electroweak phase transition (T_C), the dynamics of the plasma was governed by the interactions of the Minimal Standard Model (MSM). It is now well known that the interaction of a fermion with the thermal background in a plasma modifies the poles of the fermion propagator with respect to those at tree level. In a pioneering work [3], Weldon studied the modification of the fermion dispersion relation, i.e. poles of the fermion propagator, due to high temperature effects for a chirally invariant gauge theory (for instance, QCD or QED with massless fermions). In the same work, he showed that for a chirally invariant gauge theory with parity violation, as is the case for the $SU(2)_L \otimes U(1)_Y$ model, the dispersion relations for the right- and left-handed massless fermions are independent. This decoupling implies that the thermal effective fermion masses, defined as the energy values for zero momentum, are different.

For a parity preserving gauge theory at finite temperature, the fermion dispersion relation has two possible solutions. These solutions (branches in the phase space), both of positive energy, describe the propagation of the fermionic excitations of the plasma (quasi-particles) through the thermal medium. In the literature, these solutions are generally known as normal and abnormal branches. Each point of a branch corresponds to the energy and momentum values of a quasi-particle. The quasi-particles described by the normal branch (quasi-fermions) have the helicity equal to their chirality, while those described by the abnormal branch (quasi-holes) have the helicity opposite to their chirality. This was studied in detail by Weldon for massless quarks in QCD [4, 5] and by Pisarski for light massive fermions in QCD/QED [6]. The normal branch is so called because it becomes the ordinary fermionic branch at large momentum (large mass), k (M_f) $> gT$, where g stands for the coupling constant and M_f for the fermion mass. The abnormal branch owes its name to the fact that it appears as an additional physical solution only if temperature effects are taken into account. Quasi-particles reflect a collective behaviour of the plasma system at low momenta [7]. The collective behaviour of the quasi-holes only exists for $k < gT$, where their creation probabilities are non-zero. Moreover, the QCD/QED quasi-holes are physically possible for $M_f < gT$ and they disappear from the spectrum for $M_f \simeq T$ [6, 8].

The theoretical expectation that a cosmological electroweak phase transition [9] took place during the cooling of the early universe is motivated by the existence of the electroweak spontaneous symmetry breaking (ESSB) in the MSM and its extensions. The idea of the electroweak phase transition in the framework of the MSM allows the consideration of the two following phases. For $T > T_C$, the

gauge symmetry of the fermion fields is $SU(3)_C \otimes SU(2)_L \otimes U(1)_Y$, $\upsilon = 0$ and the plasma scenario is the electroweak unbroken phase. For $T < T_C$, the electroweak symmetry $SU(2)_L \otimes U(1)_Y$ is spontaneously broken. The gauge symmetry of the fermion fields is $SU(3)_C \otimes U(1)_{EM}$, $\upsilon \neq 0$, and the plasma scenario is the electroweak broken phase.

Fermionic excitations are present in both electroweak phases of the plasma. The spectrum of quasi-particles can be obtained from the thermal loop contribution to the fermion self-energy. The energy of the quasi-particles is of order $g_s T$. Quasi-particles, during their propagation in the plasma, scatter with the thermal medium and this phenomenon induces a damping rate γ [10]. This γ is proportional to the imaginary part of the self-energy [11]. The energy of the quasi-particles compared to γ is large and it is thus possible to speak about the existence of quasi-particles as coherent excited states. Quasi-particles have a finite lifetime $\sim 1/2\gamma$ and they can eventually turn into a new state, which is out of phase with the initial one. If the group velocity is $|\vec{v}|$, the mean free path is $|\vec{v}|/2\gamma$. The quantum spatial coherence, i.e. the phase relation between points separated by a distance $\geq |\vec{v}|/2\gamma$, is lost [2, 12]. Since we are interested in obtaining the branches which describe the quasi-particles, only the real part of the one-loop contribution to the self-energy will be calculated.

The main purpose of the present work is to compute exactly the one-loop dispersion relations for the different fermion sectors of the MSM for the following situations of the plasma: for the electroweak broken phase and for the electroweak unbroken one. We study numerically the behaviour of the normal and abnormal branches taking into account all terms in the fermion self-energy[3]. The flavour and chiral non-degeneracy of the quasi-particle spectrum is studied. Our attention is focused in the low-momentum regime where collective phenomena develop. Since mass and T corrections are considered numerically, we obtain a novel result, namely that thermal effective masses for fermions have a lower value in the broken phase than in the unbroken one. The existence of a similar shift was observed in [13] where, through a lattice calculation, it was found that thermal effective masses for massive bosons are smaller than those for massless bosons. We also confirm the particular behaviour of the branches in the broken phase found in [1, 2]: at variance with what happens in the unbroken phase, an energy gap of order M_f is obtained between the two branches that now have hyperbolic form. This behaviour is crucial for the mechanism of electroweak baryogenesis produced at the scattering of quasi-particles off the boundary created during the first order electroweak phase transition.

The T dependence for the top quark dispersion relations in the broken phase and for the neutrino dispersion relations in both phases is also studied. We

[3]By exact numerical computation of the fermion dispersion relations, we mean that we have included the leading and non-leading T corrections and the fermionic and bosonic mass corrections.

have found, for the top quark, that the thermal effective mass for two of the four branches can have negative value for $T \leq M_t$. In order to study the gauge independence of the dispersion relations, we compare one-loop computations in Feynman and Landau gauges. The dispersion relations are only gauge independent at leading order.

In section 2, we define the fermion dispersion relations for the different types of gauge theories involved in the calculations. In section 3, the generic gauge boson and scalar diagrams of Fig. 2 are calculated in the Feynman gauge and the real part of the finite temperature contribution to the fermion self-energy is given. In section 4, the Lorentz-invariant functions for quarks, charged leptons and neutrinos in the MSM are calculated and the corresponding dispersion relations in both phases are derived. In section 5, we study in detail the gauge invariance for the one-loop dispersion relations for massless and massive quarks in QCD. The results are extended to the MSM dispersion relations. Numerical results of the dispersion relation computations are presented in section 6. Our conclusions are summarized in section 7. Results about the calculation of the real part of the fermion self-energy in the Landau gauge are presented in Appendix B. In Appendix C, the Lorentz-invariant functions calculated in the Landau gauge are also presented.

2 Some useful definitions

The fermionic dispersion relations, for the different cases in which the chiral and parity symmetry are preserved or violated by a gauge theory, are presented in this section. The fermionic spectrum of the quasi-particles in a plasma is described by the branches obtained from the fermion dispersion relation, which is derived from the real part of the thermal contribution to the self-energy. The fermion self-energy is written as a linear combination of the matrices 1, $\not{K}$, $\not{u}$ and $\not{K}\not{u}$, where u^μ is the four-velocity of the plasma, with $u_\mu u^\mu = 1$, and K^μ is the fermion momentum. In the one-loop calculation, $\not{K}\not{u}$ terms are not generated and the real part of the thermal contribution to the fermion self-energy, for a gauge theory with parity and chirality violations, has the following form [3]:

$$\mathrm{Re}\,\Sigma'(K) = -\not{K}(a_L L + a_R R) - \not{u}(b_L L + b_R R) - M_I(c_L L + c_R R), \qquad (2.\ 1)$$

where $L \equiv \frac{1}{2}(1-\gamma_5)$ and $R \equiv \frac{1}{2}(1+\gamma_5)$ are the left- and right-handed chiral projectors respectively, and M_I is the fermion mass. The functions a_L, a_R, b_L, b_R, c_L and c_R are the chiral projections of the Lorentz-invariant functions a, b, c defined in the following way:

$$a = a_L L + a_R R, \qquad (2.\ 2)$$

$$b = b_L L + b_R R, \qquad (2.\ 3)$$

$$c = c_L L + c_R R. \tag{2. 4}$$

These functions depend on the Lorentz scalars ω and k defined by $\omega \equiv (K \cdot u)$ and $k \equiv [(K \cdot u)^2 - K^2]^{1/2}$.

The inverse fermion propagator is given by

$$S^{-1}(K) = \not{\mathcal{L}} L + \not{\Re} R - \Lambda_L L - \Lambda_R R, \tag{2. 5}$$

where:

$$\mathcal{L}^\mu = (1 + a_L) K^\mu + b_L u^\mu, \tag{2. 6}$$

$$\Re^\mu = (1 + a_R) K^\mu + b_R u^\mu, \tag{2. 7}$$

$$\Lambda_L = M_I (1 - c_L), \tag{2. 8}$$

$$\Lambda_R = M_I (1 - c_R). \tag{2. 9}$$

The fermion propagator follows from the inversion of (2. 5),

$$S = \frac{1}{D} \left[\left(\mathcal{L}^2 \not{\Re} - \Lambda_L \Lambda_R \not{\mathcal{L}} \right) L + \left(\Re^2 \not{\mathcal{L}} - \Lambda_L \Lambda_R \not{\Re} \right) R + \Lambda_R L \left(\mathcal{L} \cdot \Re - \Lambda_L \Lambda_R + \frac{1}{2} [\not{\mathcal{L}}, \not{\Re}] \right) L \right.$$
$$\left. + \Lambda_L R \left(\mathcal{L} \cdot \Re - \Lambda_L \Lambda_R + \frac{1}{2} [\not{\mathcal{L}}, \not{\Re}] \right) R \right]. \tag{2. 10}$$

The poles of the propagator correspond to values of ω and k for which the determinant D in (2. 10) vanishes [3],

$$D(\omega, k) = \mathcal{L}^2 \Re^2 - 2 \Lambda_L \Lambda_R (\mathcal{L} \cdot \Re) + (\Lambda_L \Lambda_R)^2 = 0. \tag{2. 11}$$

In the rest frame of the plasma $u = (1, \vec{0})$, Eq. (2. 11) leads to the fermion dispersion relation for a gauge theory with chiral and parity violations (for instance, the MSM after the ESSB):

$$\left\{ [\omega(1 + a_L) + b_L]^2 - k^2 [1 + a_L]^2 \right\} \left\{ [\omega(1 + a_R) + b_R]^2 - k^2 [1 + a_R]^2 \right\} -$$
$$2 M_I^2 (1 - c_L)(1 - c_R) \left\{ (\omega^2 - k^2)(1 + a_L)(1 + a_R) + \omega[(1 + a_L) b_R + (1 + a_R) b_L] + b_L b_R \right\}$$
$$+ M_I^4 (1 - c_L)^2 (1 - c_R)^2 = 0. \tag{2. 12}$$

Equation (2. 12) describes in a coupled way the behaviour of the left and right components. This equation is of fourth order in ω, so that for each value of k there are four solutions for ω. Therefore four branches (two normal and two abnormal) in the phase space are obtained from the dispersion relation. It is not possible to associate a specific chirality with the quasi-particles because the chiral symmetry is broken.

For massless fermions, the chiral symmetry is preserved by the theory. The functions Λ_L and Λ_R in (2. 11) are equal to zero and the poles of the propagator are found from $\mathcal{L}^2 \Re^2 = 0$. Thus, for a chirally invariant theory with parity

violation, as is the case of the MSM before the ESSB, the dispersion relations are given by

$$[\omega(1+a_L)+b_L]^2 - k^2[1+a_L]^2 = 0, \tag{2. 13}$$

$$[\omega(1+a_R)+b_R]^2 - k^2[1+a_R]^2 = 0. \tag{2. 14}$$

Left- and right-handed components now obey decoupled relations. Equations (2. 13) and (2. 14) are of second order in ω; as a consequence, for each momentum value k there are two values of ω re-solving each equation. For each fermion chirality, two branches (one normal and one abnormal) are solutions of the dispersion relation. Four branches describe the fermionic quasi-particles of the plasma. The quasi-particles have a specific chirality, in contrast with what happens in the chiral violation case.

For a parity-symmetric gauge theory, the projections of the Lorentz-invariant functions over the left- and right-handed components coincide. Setting $a_L = a_R = a$, $b_L = b_R = b$ and $c_L = c_R = c$ in (2. 12), the dispersion relation for a parity-invariant gauge theory with chirality violation (for instance, QCD with massive quarks) is obtained:

$$[\omega(1+a)+b]^2 - k^2[1+a]^2 - M_I^2[1-c]^2 = 0. \tag{2. 15}$$

The left- and right-handed components of the dispersion relation are superimposed in this case, and the fermionic excitations are only described by two branches.

If chiral symmetry is preserved by a parity-invariant gauge theory, as is the case of QCD with massless quarks, the dispersion relation is given by (2. 15), with $M_I = 0$,

$$[\omega(1+a)+b]^2 - k^2[1+a]^2 = 0. \tag{2. 16}$$

3 Real part of the fermion self-energy

The finite temperature contribution of the one-loop fermion self-energy is calculated in this section. The MSM Feynman diagrams that contribute to the one-loop fermion self-energy have the form of the generic diagrams of Figs. 1 and 2. These generic diagrams are calculated, in the Feynman gauge, using the real time formalism of thermal field theory [14]. It is straightforward to see that tadpole diagrams represented by Fig. 1 only contribute to the imaginary part of the self-energy, as is shown in Appendix A. The diagrams that contribute to the real part of the self-energy are represented by the generic diagrams of Fig. 2. To calculate the poles of the fermion propagator, we are only interested in the contribution to the real part of the fermion self-energy from these diagrams. The same calculation is also performed in the Landau gauge (Appendix B).

Finite temperature Feynman rules for vertices are the same as those in the MSM at $T = 0$, while the thermal propagators for massive fermions $S(p)$, massive gauge bosons $D_{\mu\nu}(p)$ and massive scalar bosons $D(p)$ are given by

$$S(p) = (\not{p} + M_1)\left[\frac{1}{p^2 - M_1^2 + i\epsilon} + i\Gamma_f(p)\right], \tag{3. 1}$$

$$D_{\mu\nu}(p) = -g_{\mu\nu}\left[\frac{1}{p^2 - M_2^2 + i\epsilon} - i\Gamma_b(p)\right], \tag{3. 2}$$

$$D(p) = \frac{1}{p^2 - M_2^2 + i\epsilon} - i\Gamma_b(p), \tag{3. 3}$$

where the T dependence is introduced through the functions $\Gamma_f(p)$ and $\Gamma_b(p)$ defined by

$$\Gamma_f(p) \equiv 2\pi\delta(p^2 - M_1^2)n_F(p\cdot u), \tag{3. 4}$$

$$\Gamma_b(p) \equiv 2\pi\delta(p^2 - M_2^2)n_B(p\cdot u), \tag{3. 5}$$

where $n_F(p\cdot u)$ and $n_B(p\cdot u)$ have the following form:

$$n_F(p\cdot u) = [e^{[|p\cdot u|/T]} + 1]^{-1}, \tag{3. 6}$$

$$n_B(p\cdot u) = [e^{[|p\cdot u|/T]} - 1]^{-1}. \tag{3. 7}$$

The contribution to the self-energy from the generic gauge boson diagram of Fig. 2a is

$$\Sigma(K) = ig^2 C_c \int \frac{d^4p}{(2\pi)^4} D_{\mu\nu}(p)\gamma^\mu S(p+K)\gamma^\nu, \tag{3. 8}$$

where g is the coupling constant and C_c is the quadratic Casimir invariant of the re- presentation. Inserting expressions (3. 1) and (3. 2) into (3. 8), it is possible to write: $\Sigma(K) = \Sigma^0(K) + \Sigma'(K)$, where $\Sigma^0(K)$ is the zero temperature contribution and $\Sigma'(K)$ is the finite temperature contribution. Keeping only the real part $\mathrm{Re}\,\Sigma'(K)$ of the finite temperature contribution, we obtain

$$\mathrm{Re}\,\Sigma'(K) = 2g^2 C_c \int \frac{d^4p}{(2\pi)^4}(\not{p}+\not{K}-2M_1)\left[\frac{\Gamma_b(p)}{(p+K)^2 - M_1^2} - \frac{\Gamma_f(p+K)}{p^2 - M_2^2}\right], \tag{3. 9}$$

where the denominators are defined by their principal value. Applying Weldon's procedure [3] and after performing the integrations over p_0 and the two angular variables, the following novel integrals over the modulus of the three-momentum $p = |\vec{p}|$ are obtained:

$$\frac{1}{4}Tr(\mathrm{Re}\,\Sigma') = -2g^2 C_c M_1 \int_0^\infty \frac{dp}{8\pi^2}\frac{p}{k}\left[\frac{1}{\epsilon_2}L_2^+(p)n_B(\epsilon_2) + \frac{1}{\epsilon_1}L_1^+(p)n_F(\epsilon_1)\right], \tag{3. 10}$$

$$\frac{1}{4}Tr(\not{K}\mathrm{Re}\,\Sigma') = g^2 C_c \int_0^\infty \frac{dp}{8\pi^2}\frac{p}{k}\left[\frac{1}{\epsilon_2}\left(\frac{(\omega^2-k^2-\Delta)}{2}L_2^+(p)+4pk\right)n_B(\epsilon_2)\right.$$
$$\left.+\frac{1}{\epsilon_1}\left(\frac{(\omega^2-k^2-\Delta)}{2}L_1^+(p)+4pk\right)n_F(\epsilon_1)\right], \quad (3.\ 11)$$

$$\frac{1}{4}Tr(\not{\omega}\,\mathrm{Re}\,\Sigma') = g^2 C_c \int_0^\infty \frac{dp}{8\pi^2}\frac{p}{k}\left[\left(L_2^-(p)+\frac{\omega}{\epsilon_2}L_2^+(p)\right)n_B(\epsilon_2)+L_1^-(p)n_F(\epsilon_1)\right], \quad (3.\ 12)$$

with the logarithmic functions given by

$$L_1^\pm(p) = \log\left[\frac{\omega^2-k^2-\Delta-2\epsilon_1\omega-2kp}{\omega^2-k^2-\Delta-2\epsilon_1\omega+2kp}\right] \pm \log\left[\frac{\omega^2-k^2-\Delta+2\epsilon_1\omega-2kp}{\omega^2-k^2-\Delta+2\epsilon_1\omega+2kp}\right], \quad (3.\ 13)$$

$$L_2^\pm(p) = \log\left[\frac{\omega^2-k^2+\Delta+2\epsilon_2\omega+2kp}{\omega^2-k^2+\Delta+2\epsilon_2\omega-2kp}\right] \pm \log\left[\frac{\omega^2-k^2+\Delta-2\epsilon_2\omega+2kp}{\omega^2-k^2+\Delta-2\epsilon_2\omega-2kp}\right], \quad (3.\ 14)$$

where $k = |\vec{k}|$, $\epsilon_1 = (p^2+M_1^2)^{1/2}$, $\epsilon_2 = (p^2+M_2^2)^{1/2}$, and $\Delta = M_2^2 - M_1^2$. These expressions for $M_1 = M_2 = 0$ are identical to those derived by Weldon [3] and for $M_1 \neq 0$ and $M_2 = 0$ to those derived by Petitgirard [8].

The contribution to the fermion self-energy from the generic scalar boson diagram shown in Fig. 2b has the same form as the gauge boson contribution. The factor $2g^2C_c$ in (3. 9) is replaced by $|l^2|C'_{L,R}$, where l is the Yukawa coupling constant and $C'_{L,R}$ are given in terms of the matrices of Clebsch-Gordan coefficients Γ^i. The generic scalar boson contribution for left and right chiralities is proportional to $(\Gamma^i\Gamma^{i\dagger})_{mm'} \equiv C'_L\delta_{mm'}$ and $(\Gamma^{i\dagger}\Gamma^i)_{nn'} \equiv C'_R\delta_{nn'}$ respectively [3].

The integrals (3. 10)-(3. 12) are related to (2. 1) through

$$a(\omega,k) = \frac{1}{k^2}\left[\frac{1}{4}Tr(\not{K}\mathrm{Re}\,\Sigma') - \omega\frac{1}{4}Tr(\not{\omega}\,\mathrm{Re}\,\Sigma')\right], \quad (3.\ 15)$$

$$b(\omega,k) = \frac{1}{k^2}\left[(\omega^2-k^2)\frac{1}{4}Tr(\not{\omega}\,\mathrm{Re}\,\Sigma') - \omega\frac{1}{4}Tr(\not{K}\mathrm{Re}\,\Sigma')\right], \quad (3.\ 16)$$

$$c(\omega,k) = -\frac{1}{M_I}\frac{1}{4}Tr(\mathrm{Re}\,\Sigma'), \quad (3.\ 17)$$

where the Lorentz-invariant functions $a(\omega,k), b(\omega,k)$ and $c(\omega,k)$ can be written in terms of their chiral projections, as was shown in (2. 2)-(2. 4), and M_I is the mass of the external fermion.

It is convenient to rewrite (3. 15)-(3. 17) in the following form:

$$a(\omega,k) = g^2C_cA(M_1,M_2), \quad (3.\ 18)$$

$$b(\omega,k) = g^2C_cB(M_1,M_2), \quad (3.\ 19)$$

$$c(\omega,k)=2g^2C_c\frac{M_1}{M_I}C(M_1,M_2), \tag{3. 20}$$

with

$$A(M_1,M_2)=\frac{1}{k^2}\int_0^\infty\frac{dp}{8\pi^2}\left(\left[-\frac{(\omega^2+k^2+\Delta)}{2k}\frac{p}{\epsilon_2}L_2^+(p)-\frac{\omega p}{k}L_2^-(p)+\frac{4p^2}{\epsilon_2}\right]n_B(\epsilon_2)\right.$$
$$\left.+\left[\frac{(\omega^2-k^2-\Delta)}{2k}\frac{p}{\epsilon_1}L_1^+(p)-\frac{\omega p}{k}L_1^-(p)+\frac{4p^2}{\epsilon_1}\right]n_F(\epsilon_1)\right) \tag{3. 21}$$

$$B(M_1,M_2)=\frac{1}{k^2}\int_0^\infty\frac{dp}{8\pi^2}\left(\left[\frac{(\omega^2-k^2)}{k}pL_2^-(p)+\frac{(\omega^2-k^2+\Delta)}{2}\frac{\omega}{k}\frac{p}{\epsilon_2}L_2^+(p)-\frac{4\omega p^2}{\epsilon_2}\right]n_B(\epsilon_2)\right.$$
$$\left.+\left[\frac{(\omega^2-k^2)}{k}pL_1^-(p)-\frac{(\omega^2-k^2-\Delta)}{2}\frac{\omega}{k}\frac{p}{\epsilon_1}L_1^+(p)-\frac{4\omega p^2}{\epsilon_1}\right]n_F(\epsilon_1)\right), \tag{3. 22}$$

$$C(M_1,M_2)=\frac{1}{k}\int_0^\infty\frac{dp}{8\pi^2}\left(\frac{p}{\epsilon_2}L_2^+(p)n_B(\epsilon_2)+\frac{p}{\epsilon_1}L_1^+(p)n_F(\epsilon_1)\right). \tag{3. 23}$$

Since each one-loop diagram contribution to the real part of the fermion self-energy is proportional to the generic gauge boson contribution (3. 9), it is possible to write

$$a(\omega,k)=\sum_n f_nA(M_1,M_2), \tag{3. 24}$$

$$b(\omega,k)=\sum_n f_nB(M_1,M_2), \tag{3. 25}$$

$$c(\omega,k)=\sum_n g_nC(M_1,M_2), \tag{3. 26}$$

where the Lorentz-invariant functions are obtained by adding up the contributions n coming from each diagram involved in the calculation; M_1 and M_2 refer to the internal fermion and to the boson mass of the loop diagram, respectively.

4 Fermionic dispersion relations

In this section, the one-loop dispersion relations at finite temperature for quarks, charged leptons and neutrinos in the MSM are derived. The chiral projections of the Lorentz-invariant functions in the broken and in the unbroken phases are calculated following the procedure explained in the last section. The unbroken phase Lorentz-invariant functions calculated in the Landau gauge are presented in Appendix C.

In the MSM, the W and Z gauge bosons and the fermions acquire mass after the ESSB. These masses are written as functions of υ in the form: $M_W^2=g^2\upsilon^2/4$, $M_Z^2=(g^2+g'^2)\upsilon^2/4$ and $M_F^2=l_F^2\upsilon^2/2$, where g and g' are the gauge coupling constants of $SU(2)_L$ and $U(1)_Y$ respectively and l_F is the Yukawa coupling constant

of the fermion F to the Higgs boson. The mass of the Higgs boson is $M_H^2 = \rho v^2/2$, where ρ is a free parameter of the Higgs potential. The thermal dependence of the boson and fermion masses is given through v by $v(T) \simeq v_0(1 - T^2/T_C^2)^{1/2}$, where $T_C \sim 100$ GeV is the critical temperature of the electroweak phase transition and $v_0 = 246$ GeV is the vacuum expectation value of the Higgs field at $T = 0$. The latter expression is valid for values of T near and below T_C.

4.1 Quark dispersion relations

As we have already mentioned, the damping rate of the quasi-particles in the plasma is proportional to the imaginary part of the fermion self-energy. The damping rate is induced by the incoherent scattering of the quasi-particles with the thermal medium. The scattering of the quasi-particles associated to quarks is generated by the strong and electroweak thermal interactions. The most important contribution to the damping rate comes from QCD thermal interactions. It has been calculated at leading order for zero quasi-particle momentum in [11] giving: $\gamma_{QCD} \sim 0.15 g_s^2 T$, i.e. ~ 19 GeV at $T = 100$ GeV, where g_s is the strong coupling constant.

Assuming that, in the vicinity of $k = 0$, the damping rate is not changed appreciably by the electroweak thermal interactions, the finite lifetime of the quasi-particles is $\sim 1/40$ GeV^{-1}. Since the group velocity is $\sim 1/3$, the mean free path is $\sim 1/120$ GeV^{-1}. Thus, the quantum spatial coherence is lost for points separated by a distance $\geq 1/120$ GeV^{-1}. We show below that the electroweak corrections to the branches for light quarks are of the order of the quark masses M_I. Thus, the imaginary part of the QCD self-energy is much larger than the electroweak contributions to the real part of the self-energy for all quarks but the top. This means that coherent electroweak quantum phenomena associated to quarks (for instance, CP violation) cannot take place in the plasma because the lifetime of the quasi-particles is very small with respect to the characteristic time of the electroweak processes [2, 12]. When a quasi-particle scatters, the electroweak coherence is lost.

4.1.1 Broken phase

The thermal background interacting with quarks in the plasma is constituted by massive quarks of three flavours with colour charge, massive Higgs bosons, massive W and Z gauge bosons, photons and gluons. Quarks of electric charge $2/3$ are called up quarks and those of electric charge $-1/3$ down quarks. The one-loop diagrams with photon, gluon, Z gauge boson, neutral Goldstone and Higgs boson, which contribute to the quark self-energy, do not induce a change of flavour in the quark. The diagrams with an exchange of charged Goldstone and W gauge bosons induce a flavour change in the incoming quark I to a different outgoing quark F. In the latter contributions, the flavour i of the internal quark

(inside the loop) runs over the up or down quark flavours according to the type of the external quark (outside the loop). The one-loop contribution from gauge boson and scalar boson to the real part of the self-energy gives

$$a_{\substack{L\\R}}(\omega,k)_{IF} = [fA(M_I,0)+f^Z_{\substack{L\\R}}A(M_I,M_Z)+f^H A(M_I,M_H)]\delta_{IF}+\sum_i f^W_{\substack{L\\R}}A(M_i,M_W), \tag{4. 1}$$

$$b_{\substack{L\\R}}(\omega,k)_{IF} = [fB(M_I,0)+f^Z_{\substack{L\\R}}B(M_I,M_Z)+f^H B(M_I,M_H)]\delta_{IF}+\sum_i f^W_{\substack{L\\R}}B(M_i,M_W), \tag{4. 2}$$

$$c_{\substack{L\\R}}(\omega,k)_{IF} = [2fC(M_I,0)+g^Z C(M_I,M_Z)-f^H C(M_I,M_H)]\delta_{IF}+\sum_i g^W_{\substack{L\\R}}C(M_i,M_W). \tag{4. 3}$$

The integrals (3. 21)-(3. 23) will be evaluated with the appropriate values of M_1 and M_2 for each contribution. The coefficients f_n and g_n are:

$$f = \frac{4}{3}g_s^2 + g^2Q_I^2s_w^2, \tag{4. 4}$$

$$f^Z_L = \frac{g^2}{c_w^2}(T_I^3 - Q_I s_w^2)^2 + \frac{g^2\lambda_I^2}{8}, \qquad f^Z_R = \frac{g^2}{c_w^2}Q_I^2 s_w^4 + \frac{g^2\lambda_I^2}{8}, \tag{4. 5}$$

$$f^H = \frac{g^2\lambda_I^2}{8}, \tag{4. 6}$$

$$f^W_L = \frac{g^2}{2}(1+\frac{\lambda_i^2}{2})K^+_{Ii}K_{iF}, \qquad f^W_R = \frac{g^2\lambda_I\lambda_J}{4}K^+_{Ii}K_{iF}, \tag{4. 7}$$

$$g^Z = -\frac{2g^2}{c_w^2}(T_I^3 - Q_I s_w^2)Q_I s_w^2 + \frac{g^2\lambda_I^2}{8}, \tag{4. 8}$$

$$g^W_L = \frac{g^2\lambda_i^2}{4}K^+_{Ii}K_{iF}, \qquad g^W_R = \frac{g^2\lambda_i^2\lambda_F}{4\lambda_I}K^+_{Ii}K_{iF}, \tag{4. 9}$$

where K represents the Cabibbo-Kobayashi-Maskawa (CKM) matrix, λ_I is defined as $\lambda_I = M_I/M_W$, g is the weak coupling constant, Q_I is the quark charge and s_w (c_w) is the sine (cosine) of the electroweak mixing angle θ_w. The Yukawa coupling constant l_I is related to λ_I through $l_I = g\lambda_I/\sqrt{2}$. The substitution of the expressions (4. 1)-(4. 3) in (2. 12) results in a non-diagonal matrix because of the presence of mixing in the CKM matrix. From the quark dispersion relation obtained, the branches are computed. The mass non-degeneracy of the quark spectrum and the different Yukawa coupling constants for the distinct quark flavours introduce the flavour non-degeneracy of the branches. The branches associated to each quark flavour are different because of the presence of M_I, λ_I, Q_I and the CKM matrix in (4. 1)-(4. 3).

The spectrum of quasi-particles for massive quarks with only QCD interactions was studied in [6, 8]. The quasi-particles are described by one normal and one abnormal branch. If electroweak effects are introduced, as they are here, the

mentioned spectrum is modified in a complicated way. Although the electroweak corrections are quantitatively small for all flavours but the top, some important consequences are derived from these effects. In particularly, as was explained in section 2, four branches are present (two normal and two abnormal) instead of the two QCD ones. The four branches for the s and c quarks are shown in Figs. 3 and 4. Because the chiral symmetry of the theory with massive quarks is broken, it is impossible to associate a specific chirality to the branches. The top quark acquires a large mass during the electroweak phase transition. We note a particular behaviour of the top quark branches with the T variation: a couple of branches lowers down appreciably as T is lowered (M_t increases) as is shown in Fig. 5, by means of the T variation of the thermal effective masses. To try to understand this special behaviour of the top quark branches, we will first study the much simpler QCD case.

It is very easy to check that (4. 1)-(4. 3) reduce to QCD functions when g is fixed to zero in the coefficients (4. 4)-(4. 9). That is for $a_L = a_R = a$, $b_L = b_R = b$, $c_L = c_R = c$,

$$a(\omega, k) = f' A(M_I, 0), \tag{4. 10}$$

$$b(\omega, k) = f' B(M_I, 0), \tag{4. 11}$$

$$c(\omega, k) = 2f' C(M_I, 0), \tag{4. 12}$$

where $f' = \frac{4}{3} g_s^2$. Inserting these expressions in (2. 15), the dispersion relation for massive quarks in QCD is obtained. We have checked the validity of the analytic approximations performed in [8] for light massive quarks ($M_I << T$). In this case, the analytic forms of the normal and abnormal branches for $k << T$ are:

$$\omega = M_+ + \frac{1}{M_{Lead}^2 + M_+^2} \left[\frac{M_{Lead}^2}{3M_+} + \frac{1}{2M_I} \left(\frac{3M_+^2 - M_{Lead}^2}{3M_+} \right)^2 \right] k^2 + \mathcal{O}(k^4), \tag{4. 13}$$

$$\omega = M_- + \frac{1}{M_{Lead}^2 + M_-^2} \left[\frac{M_{Lead}^2}{3M_-} - \frac{1}{2M_I} \left(\frac{3M_-^2 - M_{Lead}^2}{3M_-} \right)^2 \right] k^2 + \mathcal{O}(k^4), \tag{4. 14}$$

respectively, with $M_+ = [(M_I^2 + 4M_{Lead}^2)^{1/2} + M_I]/2$ and $M_- = [(M_I^2 + 4M_{Lead}^2)^{1/2} - M_I]/2$, where $M_{Lead}^2 = f' T^2/8$. If $k = 0$ then $\omega = M_+$ for the normal branch and $\omega = M_-$ for the abnormal branch. These different values of the energy are interpreted as thermal effective masses. For values of k close to zero, the normal branch is above $(M_I^2 + 4M_{Lead}^2)^{1/2}/2$ by $M_I/2$ while the abnormal one is below that value by the same amount. The separation between the branches is M_I and this increases with the quark mass. When the electroweak corrections are taken into account, a similar effect is also present. An energy gap of order $\sim M_I$ appears between the minimum and the maximum of the hyperbolic branches (see Figs. 3 and 4). If the quark mass is large, the energy gap is larger than the separation between the thermal effective masses. As a consequence, the

normal and abnormal branches with the same thermal effective mass appear closer. For some T, the thermal effective mass of smaller energy can be negative, as is suggested by Fig. 5.

More works about the dispersion relation for massive quarks in QCD can be found in the literature. Analytic expressions for the dispersion relation were calculated, in the limit $M_I^2 + k^2 >> M_{Lead}^2$, by Seibert [15]. In the limit $M_I^2 >> M_{Lead}^2$ as was done in [16], the approximation for the dispersion relation $\omega^2 = k^2 + M_I^2 + M_{Lead}^2$ is valid. The properties of the quark spectrum were studied by Lebedev and Smilga [17] considering a dynamical thermal mass for the quarks in the tree-level matrix Green's Functions.

4.1.2 Unbroken phase

With the masses of the particles equal to zero, the expressions (4. 1)-(4. 3) are reduced to the chiral projections of the Lorentz-invariant functions in the unbroken phase:

$$a_L(\omega,k)_{IF} = l_{IF}A(0,0), \tag{4. 15}$$

$$b_L(\omega,k)_{IF} = l_{IF}B(0,0), \tag{4. 16}$$

$$a_R(\omega,k)_{IF} = r_{IF}A(0,0), \tag{4. 17}$$

$$b_R(\omega,k)_{IF} = r_{IF}B(0,0), \tag{4. 18}$$

where the coefficients l_{IF} and r_{IF} are given by

$$l_{IF} = 8\left\{\left(\frac{2\pi\alpha_S}{3} + \frac{3\pi\alpha_W}{8}\left[1 + \frac{\tan^2\theta_W}{27} + \frac{1}{3}\lambda_I^2\right]\right)\delta_{IF} + \frac{\pi\alpha_W}{8}K_{Ii}^{+}\lambda_i^2 K_{iF}\right\}, \tag{4. 19}$$

$$r_{IF} = 8\left\{\frac{2\pi\alpha_S}{3} + \frac{\pi\alpha_W}{2}\left[Q_I^2\tan^2\theta_W + \frac{1}{2}\lambda_I^2\right]\right\}\delta_{IF}. \tag{4. 20}$$

The branches for massless quarks are computed from the dispersion relation obtained by substituting (4. 15)-(4. 18) in (2. 13) and (2. 14). Two normal branches (one left-handed and one right-handed) and two abnormal branches (one left-handed and one right-handed) describe quasi-quarks and quasi-holes respectively. The different Yukawa coupling constants for the distinct quark flavours introduce the flavour non-degeneracy of the branches. In Figs. 3 and 4, the s and c quark branches are presented.

Calculating for $\omega, k \ll T$ the leading $\mathcal{O}(T^2)$ contribution to the expressions (4. 15)-(4. 18), it is possible to observe analytically the chiral non-degeneracy of the quasi-particle spectrum. The integrals $A(0,0)$ and $B(0,0)$ in this limit allow us to write

$$a_L(\omega,k)_{IF} = \frac{1}{8}\frac{l_{IF}T^2}{k^2}\left[1 - F\left(\frac{\omega}{2k}\right)\right], \tag{4. 21}$$

$$b_L(\omega,k)_{IF} = -\frac{1}{8}\frac{l_{IF}T^2}{k}\left[\frac{\omega}{k} + (\frac{k}{w} - \frac{w}{k})F\left(\frac{\omega}{2k}\right)\right], \tag{4. 22}$$

$$a_R(\omega,k)_{IF} = \frac{1}{8}\frac{r_{IF}T^2}{k^2}\left[1 - F\left(\frac{\omega}{2k}\right)\right], \tag{4. 23}$$

$$b_R(\omega,k)_{IF} = -\frac{1}{8}\frac{r_{IF}T^2}{k}\left[\frac{\omega}{k} + (\frac{k}{w} - \frac{w}{k})F\left(\frac{\omega}{2k}\right)\right], \tag{4. 24}$$

where $F(x)$ is defined by:

$$F(x) = \frac{x}{2}\left[\log\left(\frac{x+1}{x-1}\right)\right]. \tag{4. 25}$$

In this limit, the quark self-energy has been calculated for QCD in [3, 18] and generalized for the MSM in [1]. The following analytical expressions are derived by replacing (4. 21)-(4. 24) in (2. 13) and (2. 14):

$$\omega_{L,R} - k = \frac{M_{L,R}^2}{k}\left[1 + \left[1 - \frac{\omega_{L,R}}{k}\right]\frac{1}{2}\log\left(\frac{\omega_{L,R}+k}{\omega_{L,R}-k}\right)\right], \tag{4. 26}$$

where we have defined $M_L^2 = l_{IJ}T^2/8$ and $M_R^2 = r_{IJ}T^2/8$. The normal and abnormal branches for small momentum ($k << M_{L,R}$) are given by

$$\omega_{L,R}(k) = M_{L,R} + \frac{k}{3} + \frac{k^2}{3M_{L,R}} + \mathcal{O}(k^3), \tag{4. 27}$$

$$\omega_{L,R}(k) = M_{L,R} - \frac{k}{3} + \frac{k^2}{3M_{L,R}} + \mathcal{O}(k^3), \tag{4. 28}$$

respectively. For $k = 0$, $\omega_{L,R} = M_{L,R}$ and then $M_{L,R}$ are interpreted as thermal effective masses. For each chirality, one normal and one abnormal branch describe the quasi-particle spectrum. For high momentum ($k >> M_{L,R}$), the branches are approximated by

$$\omega_{L,R}(k) = k + \frac{M_{L,R}^2}{k} - \frac{M_{L,R}^4}{2k^3}\log\left(\frac{2k^2}{M_{L,R}^2}\right) + ... \tag{4. 29}$$

$$\omega_{L,R}(k) = k + 2k\cdot\exp\left[-\frac{2k^2}{M_{L,R}^2}\right] + ... \tag{4. 30}$$

For $k >> M_{L,R}$ the branches become the ordinary fermionic branch. The leading $\mathcal{O}(g_s^2T^2)$ expressions (4. 21)-(4. 24) are gauge independent and they give place to the gauge invariant dispersion relations (4. 27)-(4. 30) [3]. Supposing that the propagation of quasi-particles is along the z axis, it is possible to see that their group velocity is of $\pm 1/3$. For k_z and a given flavour, quasi-particles of a specific chirality have two possible helicities. The group velocity is given by the eigenvalue of $\simeq 1/3\gamma_5\sigma_z = 1/3\gamma_5\sigma_z(\hat{k}_z)^2$, i.e. $1/3\chi h\hat{k}_z$, where h is twice the helicity, χ the chirality and $\hat{k}_z = k_z/|k_z|$ [2]. Consequently, the group velocity for quasi-fermions has the same sign as the momentum when chirality equals

helicity. For quasi-holes, the group velocity and the momentum have opposite signs. These fermionic states have flipped chirality/helicity and at zero T they have negative energy. They become physical at finite T due to a shift in energy of the branch.

Turning off the electroweak interactions in the Lorentz-invariant functions (4. 15)-(4. 18), the QCD case for massless quarks is recovered, with

$$a(\omega,k) = f' A(0,0), \tag{4. 31}$$

$$b(\omega,k) = f' B(0,0). \tag{4. 32}$$

The corresponding dispersion relations follow from the substitution of (4. 31) and (4. 32) in (2. 16). In the limit $\omega, k << T$ the branches are given by (4. 27) and (4. 28), with $\omega_L = \omega_R = \omega$ and $M_L = M_R = M_{Lead}$ in accordance with [3, 5, 18].

4.2 Charged-lepton dispersion relations

The scattering between the quasi-particles associated to charged leptons and the thermal medium is governed by the weak and electromagnetic thermal interactions. It is expected for $k = 0$, in analogy with QCD calculations [11], that the damping rate at leading order originated only from weak or electromagnetic thermal interactions were $\gamma_{EW} \sim g^2 T$. The weak and electromagnetic leading contributions of the real part of the self-energy are both of order gT. This means that the energy of the quasi-particles, of order gT, is large in comparison with the damping rate, i.e. it contains one additional power of g. Thus, it is possible to speak of the existence of quasi-particles as coherent excited states. Coherent electroweak quantum phenomena associated to charged leptons can take place in the plasma because the lifetime of the quasi-particles is of the order of the characteristic time of the electroweak processes.

4.2.1 Broken phase

The thermal background interacting with charged leptons in the plasma is constituted by massive charged leptons of flavour e, massless neutrinos of flavour e, massive Higgs bosons, massive W and Z gauge bosons and massless photons. The diagrams with charged Goldstone and W bosons change from the external charged lepton to the associated neutrino flavour inside the loop. The one-loop contribution from scalar and gauge boson sectors to the real part of self-energy allow us to write

$$a_{\substack{L\\R}}(\omega,k) = dA(M_e,0) + d^Z_{\substack{L\\R}} A(M_e,M_Z) + d^H A(M_e,M_H) + d^W_{\substack{L\\R}} A(0,M_W), \tag{4. 33}$$

$$b_{\substack{L\\R}}(\omega,k) = dB(M_e,0) + d^Z_{\substack{L\\R}} B(M_e,M_Z) + d^H B(M_e,M_H) + d^W_{\substack{L\\R}} B(0,M_W), \tag{4. 34}$$

$$c_L(\omega,k) = c_R(\omega,k) = 2dC(M_e,0) + y^Z C(M_e,M_Z) - d^H C(M_e,M_H), \tag{4. 35}$$

with the coefficients d and y given by

$$d = g^2 s_w^2, \tag{4. 36}$$

$$d_L^Z = \frac{g^2}{c_w^2}(\frac{1}{2} - s_w^2)^2 + \frac{g^2\lambda_e^2}{8}, \qquad d_R^Z = \frac{g^2}{c_w^2}s_w^4 + \frac{g^2\lambda_e^2}{8}, \tag{4. 37}$$

$$d^H = \frac{g^2\lambda_e^2}{8}, \tag{4. 38}$$

$$d_L^W = \frac{g^2}{2}, \qquad d_R^W = \frac{g^2\lambda_e^2}{4}, \tag{4. 39}$$

$$y^Z = -\frac{2g^2}{c_w^2}(\frac{1}{2} - s_w^2)s_w^2 + \frac{g^2\lambda_e^2}{8}, \tag{4. 40}$$

where $\lambda_e = M_e/M_W$. Substituting the functions (4. 33)-(4. 35) in (2. 12), the branches are computed from the obtained dispersion relation. Because the chiral symmetry in this case is broken, it is impossible to associate a specific chirality to the branches. Flavour non-degeneracy exists since the mass non-degeneracy is present in (4. 33)-(4. 35).

The spectrum of quasi-particles for charged leptons in QED was studied in [19]. For this case, the quasi-particles are described by one normal and one abnormal branch, and left- and right-handed branches are superposed. The breaking of the parity symmetry by the weak interactions causes the doubling of the QED branches. Thus, for charged leptons in the MSM, the quasi-particles are described by two normal and two abnormal branches, as is shown in Fig. 6 for the τ lepton. As in the quark case in the broken phase, an energy gap between the hyperbolic branches appears.

Following a procedure analogous to the one performed for massive quarks in QCD, the Lorentz-invariant functions for massive electrons in the QED case are obtained by turning off the weak interactions into the functions (4. 33)-(4. 35). The expressions derived are similar to expressions (4. 10)-(4. 12), with f' changed to d and M_I to M_e. The analytic form of the two branches, for $k << T$, is given by (4. 13) and (4. 14).

Some aspects of the dispersion relation for massive electrons in QED have been studied at finite temperature, considering an effective chemical potential in [20, 21]. The spectrum of quasi-particles in a hot relativistic electron plasma was studied in [22], where it is shown numerically that the full spectral weight is not gauge independent. By comparing one-loop computations in the Feynman and in the Coulomb gauges, it was shown in [22] that the location of well-defined poles in the propagator is gauge independent at leading order since the poles correspond to physical excitations, while the widths of the quasi-particles are gauge dependent. The dispersion relation at zero temperature has been studied in [23].

4.2.2 Unbroken phase

Expressions (4. 33)-(4. 35) with particle masses equal to zero reduce to the chiral projections of the Lorentz-invariant functions in the unbroken phase:

$$a_L(\omega, k) = tA(0,0), \tag{4. 41}$$

$$b_L(\omega, k) = tB(0,0), \tag{4. 42}$$

$$a_R(\omega, k) = uA(0,0), \tag{4. 43}$$

$$b_R(\omega, k) = uB(0,0), \tag{4. 44}$$

where the coefficients t and u are

$$t = \pi\alpha_W \left[2 + \frac{1}{c_w^2} + \lambda_e^2\right], \tag{4. 45}$$

$$u = 4\pi\alpha_W \left[\tan^2\theta_W + \frac{\lambda_e^2}{2}\right]. \tag{4. 46}$$

The branches for massless charged leptons are computed from the dispersion relation derived by substituting (4. 41)-(4. 44) in (2. 13) and (2. 14). Two normal branches (one for each chirality) and two abnormal branches (one for each chirality) describe quasi-particles and quasi-holes respectively (see Fig. 6). The quasi-particle spectrum is flavour non-degenerate, but, because λ_e^2 in (4. 45) and (4. 46) is so small for all charged lepton flavours, the differences between flavours are very small. The type of quasi-particle characterized by the abnormal branch has been called the "plasmino" by Braaten and Pisarski [24]. In the limit $\omega, k \ll T$, the analytical forms obtained for the dispersion relation are similar to those obtained for massless quarks. For $k << M_{L,R}$, the branches are given by (4. 27) and (4. 28) with $M_L^2 = tT^2/8$ and $M_R^2 = uT^2/8$.

4.3 Neutrino dispersion relations

The damping rate of quasi-particles associated to neutrinos is induced by the weak thermal interactions. In analogy with the assumption in the charged-lepton case, the damping rate (leading order) of neutrino quasi-particles for $k = 0$ is $\gamma_{EW} \sim g^2T$. The weak leading contribution of the real part of the self-energy is of order gT. The energy of the quasi-particles, of order gT, compared to the damping rate is large. The quasi-particles exist as coherent excited states. Coherent weak quantum phenomena associated with neutrinos can take place in the plasma because the lifetime of the quasi-particles is of the order of the characteristic time of the weak processes.

4.3.1 Broken phase

The thermal background interacting with neutrinos in the plasma is constituted by massless neutrinos of flavour e, massive charged leptons of flavour e and massive W and Z gauge bosons. The one-loop contribution from scalar and gauge boson sectors to the real part of the self-energy lead to

$$a_L(\omega, k) = v_Z A(0, M_Z) + v_W A(M_e, M_W), \tag{4. 47}$$

$$b_L(\omega, k) = v_Z B(0, M_Z) + v_W B(M_e, M_W), \tag{4. 48}$$

with the coefficients v_Z and v_W given by

$$v_Z = \frac{\pi \alpha_W}{c_w^2}, \tag{4. 49}$$

$$v_W = \pi \alpha_W [2 + \lambda_e^2], \tag{4. 50}$$

where $\lambda_e = M_e/M_W$. The projection of the Lorentz-invariant functions is only over the left-handed component. Substituting (4. 47) and (4. 48) in (2. 13), the branches are computed from the dispersion relation obtained. A normal and an abnormal branches of left-handed chirality describe the quasi-particles as is shown in Fig. 7. Flavour non-degeneracy exists from the mass non-degeneracy present in (4. 47) and (4. 48), for different neutrino flavours. Because $M_e << M_W$ in the integrals of (4. 47) and (4. 48), the differences for different flavours are very small.

The neutrino dispersion relation presented here was studied by D'Olivo, Nieves and To- rres in [25] for temperatures of the plasma much lower than the W and Z masses. This approximation allows to neglect the thermal dependence for the gauge boson propagators. These authors performed the calculation in a general gauge and they found that the neutrino self-energy depends on the gauge parameter, but the dispersion relation is independent at leading order in g^2/M_W^2. Several works, previous to [25], on this subject can be found in the literature. In [26, 27], the same calculation was performed but using the unitary gauge. The computation of the neutrino thermal self-energy was considered in [28, 29].

4.3.2 Unbroken phase

Expressions (4. 47) and (4. 48) with gauge boson masses equal to zero reduce to the left-handed projection of the Lorentz-invariant functions in the unbroken phase:

$$a_L(\omega, k) = tA(0, 0), \tag{4. 51}$$

$$b_L(\omega, k) = tB(0, 0), \tag{4. 52}$$

with the coefficient t given by (4. 45). Substituting (4. 51) and (4. 52) in (2. 13), the branches are computed from the dispersion relation obtained. A normal

and an abnormal branch of left-handed chirality describe the quasi-particles (see Fig. 7). The quasi-particle spectrum is flavour non-degenerate, but, since λ_e^2 is very small for all neutrino flavours, the differences for the different flavours are very small. The variation with the temperature of the thermal effective masses for both phases is presented in Fig. 8.

The branches for left-handed neutrinos are the same as those for left-handed charged leptons. This result reflects the presence of the $SU(2)_L$ symmetry in the MSM before the ESSB. The neutrino dispersion relation in the unbroken phase was considered with a non-zero chemical potential in [30]. The same authors in a later work [31] studied the dispersion relation in the case where the charged leptons have a running mass obtained using the renormalization group equations.

5 Remarks about gauge invariance

The gauge invariance of the one-loop dispersion relations presented in this work is studied in this section. The numerical results for the dispersion relations have been obtained considering all the terms in the Lorentz-invariant functions (3. 18)-(3. 20). This fact implies the introduction of a small gauge dependence originated from the non-leading order terms of the fermion self-energy [32]. These, in turn, lead to sub-leading contributions to the dispersion relations. Indeed, by confronting QCD computations in the Feynman and Landau gauges, we show that the sub-leading contributions to the dispersion relations are gauge dependent. We also study the effect of these contributions in our numerical results.

In Appendix B, we calculate the finite temperature contribution to the one-loop real part of the fermion self-energy in the Landau gauge $\mathrm{Re}\,\Sigma'^{\pounds}(K)$. We show in (B. 4) that it is possible to write: $\mathrm{Re}\,\Sigma'^{\pounds}(K) = \mathrm{Re}\,\Sigma'(K) + \mathrm{Re}\,\delta\Sigma'(K)$, where $\mathrm{Re}\,\Sigma'(K)$ is the real part of the thermal contribution to the self-energy in the Feynman gauge (3. 8) and $\mathrm{Re}\,\delta\Sigma'(K)$ is the real part of the gauge dependent thermal contribution of $\mathrm{Re}\,\Sigma'^{\pounds}(K)$ (B. 5). The Ward identities ensure that the gauge dependent contribution disappears if the external leg is projected on the zeroth order pole [32]. This can easily be seen because $\mathrm{Re}\,\delta\Sigma'(K)$ can be written as proportional to $\not{K} - M_q$. In QCD at finite temperature, for instance, the shift of the quark propagator pole position with respect to the pole position at zero temperature is of order $g_s T$. This means that the argument of the integral in (B. 5) is proportional to $g_s T$, for this case, because this integral is proportional to $\not{K} - M_q$. Consequently, the $\mathrm{Re}\,\delta\Sigma'(K)$ contribution to the dispersion relation is of a higher order in g_s with respect to the $\mathrm{Re}\,\Sigma'(K)$ contribution.

For example, in the QCD case for massless quarks, $\mathrm{Re}\,\delta\Sigma'(K)$ vanishes on the zeroth order pole corresponding to $\omega = 0$, for $k = 0$. So, $\mathrm{Re}\,\delta\Sigma'(K)$ contribution is a non-leading order in ω/T. These non-leading order contributions lead to a sub-leading contributions to the thermal effective mass. This fact can be guessed because the leg projection on the first order pole means $\omega/T \sim g_s$.

This conclusion is in accordance with [32], where it is formally shown that non-leading contributions to the quark self-energy allow gauge dependent sub-leading modifications to the dispersion relation.

Let us now show in an explicit calculation that the non-leading contributions to the one-loop QCD self-energy are sub-leading in the dispersion relations. By comparing one-loop computations in the Feynman and in the Landau gauge for massless and for massive quarks, we will show that indeed the sub-leading contributions to the dispersion relations are gauge dependent. First, we consider massless quarks in QCD. The Lorentz-invariant functions in the Feynman gauge (3. 18) and (3. 19) for this case are

$$a^Q(\omega,k) = \frac{M^2_{Lead}}{k^2}\left[1 - F\left(\frac{\omega}{2k}\right)\right] + \frac{A^2}{k^3}\left[\omega^2 I_1 + k^2 I_2 - 2\omega I_3\right], \qquad (5.\ 1)$$

$$b^Q(\omega,k) = \frac{M^2_{Lead}}{k}\left[\frac{\omega}{k} + (\frac{k}{\omega} - \frac{\omega}{k})F\left(\frac{\omega}{2k}\right)\right] + 2A^2\frac{\omega^2 - k^2}{k^3}\left[I_3 - \frac{\omega}{2}I_1\right], \qquad (5.\ 2)$$

where $M^2_{Lead} = g_s^2 T^2/6$, $A^2 = g_s^2/12\pi^2$ and g_s stands for the strong coupling constant. The function $F(x)$ is defined by (4. 25) and the integrals I_1, I_2, I_3 are given by

$$I_1(\omega,k,T) = \int_0^\infty dp\ L_I^+(p)\left[n_B(p) + n_F(p)\right], \qquad (5.\ 3)$$

$$I_2(\omega,k,T) = \int_0^\infty dp\ L_I^+(p)\left[n_B(p) - n_F(p)\right], \qquad (5.\ 4)$$

$$I_3(\omega,k,T) = \int_0^\infty dp\ pL_I^+(p)\left[n_B(p) + n_F(p)\right], \qquad (5.\ 5)$$

where $n_B(p)$ and $n_F(p)$ are defined by (3. 6) and (3. 7) respectively. The logarithmic functions $L_I^\pm(p)$ are

$$L_I^\pm(p) = \log\left[\frac{2p - (\omega - k)}{2p - (\omega + k)}\right] \pm \log\left[\frac{2p + (\omega + k)}{2p + (\omega - k)}\right]. \qquad (5.\ 6)$$

Substituting the expressions (5. 1) and (5. 2) into (2. 16), it follows that

$$k^2 = M^2_{Lead}\left(\frac{k}{\omega - k} - \frac{1}{2}\log\left[\frac{\omega + k}{\omega - k}\right]\right) - A^2\left(\omega I_1 - kI_2 - 2I_3\right). \qquad (5.\ 7)$$

For $k \to 0$, the integrals I_1, I_2, I_3 can be written as $I_i(\omega,k,T) = kF_i(\omega,T) + \mathcal{O}(k^3)$, where $i = 1,2,3$. The reason of this is that (5. 3)-(5. 5) are antisymmetric for the change $k \to -k$. It was not possible for us to obtain analytic expressions for the integrals (5. 3)-(5. 5). They were computed numerically for different values of ω, k and T, in the limit $k \to 0$. By means of a fit of the numerical results obtained, we have found an analytical form for the integrals. Numerically we have proved that $(\omega I_1 - 2I_3) = \mathcal{O}(k^3)$, i.e. $(\omega F_1 - 2F_3) = 0$. For this reason

$(\omega I_1 - 2I_3)$ vanishes in (5. 7), when we take the limit $k << \omega$, $T > \omega$, divide by k^2 and set $k = 0$. Then, we obtain the following relation:

$$\omega^2 \left[1 - A^2 F_2(\omega, T)\right] = M_{Lead}^2, \tag{5. 8}$$

where[4]

$$F_2(\omega, T) = 2\gamma_E + 2\log\frac{\omega}{2T}, \tag{5. 9}$$

with $\gamma_E = 0.5772$. We note that (5. 8) reduces to the leading thermal effective mass $\omega = M_{Lead}$, if the non-leading contributions given through $F_2(\omega, T)$ are set to zero. The numerical solution of (5. 8) leads to the thermal effective mass

$$M = M_{Lead}(1 + \rho), \tag{5. 10}$$

where $\rho = 0.02223$. The massless quark dispersion relations, for the limit $k << M$, are

$$\omega(k) = M + \frac{k}{3} + \frac{k^2}{3M} + \mathcal{O}(k^3), \tag{5. 11}$$

$$\omega(k) = M - \frac{k}{3} + \frac{k^2}{3M} + \mathcal{O}(k^3), \tag{5. 12}$$

where M is given by (5. 10). For the limit $k >> M$, the dispersion relations are written as (4. 29) and (4. 30), with $M_{L,R}^2 = M^2$. The inclusion of non-leading contributions leads to increase M_{Lead} by 2.223%. We have checked the validity of expressions (5. 11) and (5. 12) by comparing the results obtained from them with the results obtained by means of the exact numerical solution of the dispersion relations. The relative error of the results obtained from (5. 11) and (5. 12) is smaller than 0.01% with respect to the exact numerical results. Given the fit (5. 10), the solution of (5. 8) can be well approximated by

$$\omega = M_{Lead}\left[1 - 2A^2\left(\gamma_E + \log\left[\frac{M_{Lead}}{2T}\right]\right)\right]^{-1/2}. \tag{5. 13}$$

Expanding the root square in (5. 13), we can see that the non-leading terms of the quark self-energy modify M_{Lead} as $\propto g_s^{(n)}T$, with $(n = 3, 5, ...)$, in accordance with the conclusions given in [32].

The Lorentz-invariant functions in the Landau gauge are

$$a^{\pounds}(\omega, k) = \frac{4}{3}g_s^2[A(0,0) + A_0^{\delta}(0,0)], \tag{5. 14}$$

$$b^{\pounds}(\omega, k) = \frac{4}{3}g_s^2[B(0,0) + B_0^{\delta}(0,0)], \tag{5. 15}$$

[4]The analytical form found for I_2, for $\omega \simeq T/2$, fits the numerical solutions with a precision smaller than 0.01%.

where $A(0,0)$ and $B(0,0)$ are given by (3. 21) and (3. 22) with $M_1 = M_2 = 0$. The integrals $A_0^\delta(0,0)$ and $B_0^\delta(0,0)$ are given by (B. 9) and (B. 10) with $M_1 = 0$. Substituting (5. 14) and (5. 15) into (2. 16), we compute the quark dispersion relations in the Landau gauge. These dispersion relations coincide with those at leading order $\mathcal{O}(g_sT)$ in the Feynman gauge, as is shown in Fig. 9. In other words, the Lorentz-invariant functions (5. 14) and (5. 15) reduce to the analytical form of (4. 21) and (4. 22) with $L_{I,F} = 4g_s^2/3$. This means that non-leading contributions of $A(0,0)$ and $B(0,0)$ in (5. 14) and (5. 15) are canceled exactly by $A_0^\delta(0,0)$ and $B_0^\delta(0,0)$ contributions, respectively. For $k << \omega$, we have analytically proved this fact. For the Landau gauge, the gauge dependent parameter ρ in (5. 10) is zero. This result indicates that the one-loop dispersion relations are only gauge invariant at leading order $\mathcal{O}(g_sT)$ [3, 33]. As the thermal imaginary part of the one-loop self-energy contains only non-leading terms, it is highly gauge dependent. For a consistent calculation of this part, it is necessary to go to the imaginary time formalism of the thermal field theory and to use Pisarski's method for resumming thermal loops [11, 34].

We will now study the massive quark case in QCD. The Lorentz-invariant functions in the Feynman gauge (3. 18)-(3. 20) contain terms dependent of M_q . For the case $M_q << \omega$, it is possible to neglect[5] M_q in the logarithmic integrals, following the same arguments as given in [8].

We can write (3. 18)-(3. 20) for $M_q << \omega$ as

$$a(\omega,k) = a^Q(\omega,k) + A^2\frac{M_q^2}{k^2}\left[2\left(\log\left[\frac{M_q}{\pi T}\right] + \gamma_E\right) - \frac{1}{k}I_2\right], \tag{5. 16}$$

$$b(\omega,k) = b^Q(\omega,k) + A^2\frac{M_q^2}{k^2}\left[2\left(\log\left[\frac{M_q}{\pi T}\right] + \gamma_E\right) - \frac{1}{k}I_2\right], \tag{5. 17}$$

$$c(M_q,0) = -4A^2\frac{1}{k}I_2, \tag{5. 18}$$

where $a^Q(\omega,k)$ and $b^Q(\omega,k)$ are the Lorentz-invariant functions for the massless case (5. 1) and (5. 2), and I_2 is given by (5. 4). Substituting (5. 16)-(5. 18) in (2. 15), taking the limits $k << \omega$, $M_q << \omega$, and setting $k = 0$, we obtain the following relation:

$$\omega^2\left[1 - A^2F_2(\omega,T)\right] - M_{Lead}^2 = \omega M_q\left[1 - 4A^2F_2(\omega,T)\right], \tag{5. 19}$$

where $F_2(\omega,T)$ is given by (5. 9). This relation for $M_q = 0$ reduces to (5. 8). If non-leading contributions manifested by means of $F_2(\omega,T)$ are set to zero, the relation (5. 19) leads to the leading thermal effective masses $M_\pm$ defined in (4. 13) and (4. 14).

[5]We have numerically proved that neglecting the quark mass in the logarithmic integrals, for $M_q < \omega/20$, leads to relative errors in the integrals smaller than 0.1%.

Taking into account the validity of (5. 19) only for $M_q << M_{Lead}$, we obtain through a fit of the numerical solutions of (5. 19), that

$$M_{\pm}(M_q) = M_{Lead}\left(1+\rho\left[1-\frac{M_q}{2T}\right]\right) \pm \frac{M_q}{2}\left(1-\sigma\left[1\mp\frac{M_q}{2T}\right]\right), \qquad (5.\ 20)$$

where $\rho = 0.02223$ and $\sigma = 0.135$. For $M_q = 0$, (5. 20) reduces to (5. 10). The dispersion relations given by (4. 13) and (4. 14), with $M_{\pm}$ defined by (5. 20), contain all T contributions from the one-loop self-energy. We have also checked the validity of these analytical dispersion relations by comparing the results obtained from them with those obtained sol- ving numerically the dispersion relations. For $M_q < M_{Lead}/20$, the relative error is smaller than 0.01%.

The Lorentz-invariant functions in the Landau gauge for massive quarks in QCD are given by

$$a^{\pounds}(\omega,k) = \frac{4}{3}g_s^2[A(M_q,0) + A_0^{\delta}(M_q,0)], \qquad (5.\ 21)$$

$$b^{\pounds}(\omega,k) = \frac{4}{3}g_s^2[B(M_q,0) + B_0^{\delta}(M_q,0)], \qquad (5.\ 22)$$

$$c^{\pounds}(\omega,k) = \frac{5}{2}\frac{4}{3}g_s^2 C(M_q,0), \qquad (5.\ 23)$$

where $A(M_q,0)$, $B(M_q,0)$ and $C(M_q,0)$ are defined by (3. 21)-(3. 23), with $M_2 = 0$. $A_0^{\delta}(M_q,0)$ and $B_0^{\delta}(M_q,0)$ are defined by (B. 9) and (B. 10), respectively. The quark dispersion relations in the Landau gauge are computed inserting (5. 21)-(5. 23) into (2. 15). These dispersion relations coincide with those obtained at leading order in the Feynman gauge, as is shown in Fig. 10. The gauge dependent parameters ρ and σ in (5. 20) are zero in the Landau gauge computation; consequently, the massive quark dispersion relations are gauge invariant at leading order in temperature $\mathcal{O}(g_sT)$ and in mass $\mathcal{O}(M_q)$.

The inclusion of the non-leading one-loop contributions changes the leading thermal effective masses according to the quark mass. For instance, the change in the leading thermal effective masses for the c quark at $T = 100$ GeV are: $\delta M_+ = 0.0202 M_+$ and $\delta M_- = 0.0241 M_-$. For the s quark, they are: $\delta M_+ = 0.0220 M_+$ and $\delta M_- = 0.0224 M_-$. Thus, the effect of the sub-leading contributions to the dispersion relations is nearly 2% for the light quarks. We have not obtained a similar fit of the thermal effective masses as (5. 20) for the heavy quark case. We have checked numerically for this case that the sub-leading contributions to the thermal effective mass are small in comparison with the leading contributions.

For the MSM dispersion relations in the unbroken phase, the situation is quite similar to the QCD case for massless quarks. For instance, the thermal effective masses including leading and non-leading contributions in the Feynman gauge are given by (see Eq. (5. 10)):

$$M_{L,R}^{u} = M_{L,R}^{u(Lead)}(1+\rho), \qquad (5.\ 24)$$

being $M_{L,R}^{u(Lead)}$ the leading contribution to the thermal effective masses in the unbroken phase

$$M_{L,R}^{u(Lead)} = \sqrt{\bar{f}_{L,R}^{u} \frac{T^2}{8}}, \tag{5. 25}$$

with $\bar{f}_{L,R}^{u} = f + f_{L,R}^{Z} + f_H + f_{L,R}^{W}$, where the coefficients f_n are given by Eqs. (4. 4)-(4. 7). The Lorentz-invariant functions in the Landau gauge for this case are presented in the Appendix C. The dispersion relations in the Landau gauge coming from substituting (C. 1) and (C. 2) in (2. 13) and (2.14). In a similar way as the QCD case, the branches in the Landau gauge are superimposed on the Feynman gauge branches at leading order. In consequence, the fermion dispersion relations in the unbroken phase are gauge invariant at leading order. The consideration of all terms in the quark self-energy introduces a small gauge dependence in the dispersion relations. Taking into account (5. 24), the sub-leading contribution to the thermal effective mass in the Feynman gauge is

$$\delta M_{L,R}^{u} = \rho M_{L,R}^{u(Lead)}, \tag{5. 26}$$

where $\rho \simeq 0.023$ for this case. This contribution induces a gauge dependence in our numerical computations of nearly 2%. By the mentioned general considerations this sub-leading contribution is of order $\sim g_s^3 T$ in a general gauge.

The results obtained for massive quarks in QCD can be extended to the MSM in the broken case. The quark dispersion relations are gauge invariant at leading order in temperature and in quark mass. The non-leading order terms in the quark self-energy introduce a small gauge dependence in the dispersion relations. We have checked numerically that the thermal effective masses in the broken phase $M_{L,R}^{b}$ can be written as:

$$M_{L,R}^{b} = \frac{M_{+}^{b}(M_q)_{L,R} + M_{-}^{b}(M_q)_{L,R}}{2}, \tag{5. 27}$$

where taking into account (5. 20), $M_{\pm}^{b}(M_q)_{L,R}$ are given by:

$$M_{\pm}^{b}(M_q)_{L,R} = M_{L,R}^{b(Lead)} \left(1 + \rho \left[1 - \frac{M_q}{2T}\right]\right) \pm \frac{M_q}{2} \left(1 - \sigma \left[1 \mp \frac{M_q}{2T}\right]\right), \tag{5. 28}$$

with $\sigma \simeq 0.14$, and $M_{L,R}^{b(Lead)}$ are the thermal effective masses at leading order in the broken phase

$$M_{L,R}^{b(Lead)} = \sqrt{\bar{f}_{L,R}^{b} \frac{T^2}{8}}, \tag{5. 29}$$

where the coefficients are given by

$$\bar{f}_{L,R}^{b} = f + (1 - x_Z) f_{L,R}^{Z} + (1 - x_H) f_H + (1 - x_W) f_{L,R}^{W}. \tag{5. 30}$$

In this equation x_Z, x_H, x_W denote the effect of the boson mass contributions on the thermal effective masses, being $0 < x_Z,\, x_H,\, x_W << 1$. This fact permits

to understand why the thermal effective masses in the broken phase $M^b_{L,R}$ are smaller than those in the unbroken phase $M^u_{L,R}$. The sub-leading contribution to the thermal effective masses in the Feynman gauge, taking into account (5. 27), is

$$\delta M^b_{L,R} = \rho M^{b(Lead)}_{L,R} \left[1 - \frac{M_q}{2T}\right] + \sigma \frac{M_q^2}{4T}, \qquad (5.\ 31)$$

inducing a gauge dependence in our numerical computations about 2% for the light quarks. Due the mentioned general grounds, the sub-leading contribution to the thermal effective masses is of order $\sim g_s^3[T - M_q]$ for quarks, and of order $\sim g^3[T - M_e]$ for charged leptons and neutrinos in a general gauge.

It is easy to prove that the gauge dependence induced in the shift of the thermal effective masses between the two phases is smaller than the one mentioned above. The difference between the gauge dependent contributions to the thermal effective masses in a general gauge is of order $\sim g_s^3 M_q$ for quarks and of order $\sim g^3 M_e$ for charged leptons and neutrinos. For the light quark case, the difference in the Feynman gauge is:

$$\delta M^b_{L,R} - \delta M^u_{L,R} \simeq -\rho M^{b(Lead)}_{L,R} \frac{M_q}{2T} + \sigma \frac{M_q^2}{4T}. \qquad (5.\ 32)$$

This gauge dependence is smaller than (5. 26) and (5. 31).

6 Numerical results

We now give the numerical results we have obtained for the dispersion relations for up quarks (u, c, t), down quarks (d, s, b), charged leptons (e, μ, τ) and neutrinos $(\nu_e, \nu_\mu, \nu_\tau)$. For $T = 100$ GeV, the following values for the masses in GeV have been used: $M_W = 52$, $M_Z = 59$, $M_H = 100$, $M_d = 0.006$, $M_s = 0.09$, $M_b = 2.9$, $M_u = 0.003$, $M_c = 1.0$, $M_t = 114.7$, $M_e = 0.0003$, $M_\mu = 0.069$, $M_\tau = 1.176$ and massless neutrinos. As we have mentioned, we are specially interested in the low-momentum regime where the collective behaviour is present. Adequate boson and fermion mass values for each temperature have been used, for the cases where the thermal dependence has been studied. The values of the coupling constants have been fixed to $\alpha_s = 0.1$, $\alpha_w = 0.035$ for all temperatures.

In Figs. 3 and 4, we show the branches for quarks s and c respectively in both phases. In the unbroken phase, the left-handed branches are above the right-handed ones. Although the branches in the broken phase are not associated to a specific chirality, the number of branches is also four. While in the unbroken phase the left-handed abnormal branch is crossed by the right-handed normal branch, in the broken phase there is not crossing between the branches. In the broken phase, the branches that now have a hyperbolic form are separated between the minimum and the maximum by an energy gap of order $\sim M_f$. The quasi-particle excitations cannot exist in this energy range.

The branches for each quark flavour are different in the broken phase and clearly the fermionic spectrum described by them is flavour non-degenerate. In the unbroken phase, the left-handed branches for the different quark flavours are numerically the same in our computation, but a very small difference should exist for them. The fermionic spectrum is flavour non-degenerate, but the differences for different flavours are very small. The fermionic spectrum described by the right-handed branches is also flavour non-degenerate in a similar way to the left-handed fermionic spectrum.

Since temperature and mass corrections are considered, the thermal effective masses in the broken phase are smaller than those in the unbroken phase. For the s quark case, for instance (see Fig. 3), the thermal effective mass of the left-handed branches in the unbroken phase is $\simeq 51.4$ GeV, while that for the corresponding branches in the broken phase is $\simeq 50.0$ GeV. The shift of the thermal effective masses for the lower branches is also present, but is smaller. In our perturbative calculation, this effect can be understood through the presence of the massive boson propagator (3. 2) in the fermion self-energy. This discontinuity of the thermal effective masses between the two sides of the boundary created during the first order electroweak phase transition has recently been noted in [13]. In this reference, using a numerical simulation of the phase transition in the SU(2) Higgs model on the lattice, was found that the thermal effective mass for the W and Higgs boson is smaller in the broken phase than in the unbroken one.

The dependence with T of the top quark thermal effective masses for the branches in the broken phase is presented in Fig. 5. Two branches go down appreciably as the temperature is lowered (M_t increases). For T below 120 GeV, these branches can become unphysical as is suggested by this figure.[6] The special behaviour of the top quark branches is obtained because this quark acquire a large mass during the electroweak phase transition.

The branches for the τ lepton are shown in Fig. 6. An energy gap between the hyperbolic branches in the broken phase is also present. As in the quark case, the thermal effective masses for charged leptons in the broken phase are smaller than those in the unbroken one. In the broken phase, the branches for each flavour are different and consequently the fermionic spectrum is flavour non-degenerate. In the unbroken phase, the branches of a specific chirality are the same for different flavours within the precision of the present computation. The fermionic spectrum described is flavour non-degenerate, but the differences for different flavours are very small.

The branches for the electron neutrino are shown in Fig. 7. There are only two branches because the left-handed chirality of the neutrino. In both phases, the branches for different flavours are the same in our computations. However, the

[6]Because of numerical problems, it was not possible to obtain results for the branches for $T < 155$ GeV.

fermionic spectrum is flavour non-degenerate, in both phases, but the differences are very small for different flavours. The thermal effective masses for neutrinos in the broken phase are smaller than those in the unbroken one. The T dependence of the electron neutrino thermal effective mass is presented in Fig. 8. The thermal effective mass is zero for $T = 0$, as can be concluded from this figure.

7 Conclusions

One-loop dispersion relations for the different fermionic sectors of the MSM were obtained. The calculation was performed in the real time formalism of the thermal field theory, in the Feynman gauge. Numerical results were presented for temperatures of the plasma near the critical one of the electroweak phase transition. For all the fermions in the broken phase and in the unbroken one, the fermionic spectrum described by the branches of the dispersion relations is flavour non-degenerate.

In the unbroken phase, the fermionic quasi-particles can be associated to a specific chirality because the chiral symmetry is preserved by the MSM before the ESSB. Since the chiral symmetry is violated by the MSM after the ESSB, the quasi-particles cannot be associated to a specific chirality in the broken phase for the case of massive fermions. The number of branches for quarks and charged leptons is four in both phases, while it is only two for neutrinos.

The thermal effective masses for all fermions in the broken phase are smaller than those in the unbroken one. The existence of this shift for the thermal effective masses can be understood through the presence of the massive boson propagators in the fermion self-energy. A similar shift for the W and Higgs boson thermal effective mass has recently been observed in [13], but through a non-perturbative lattice calculation. For quarks and charged leptons in the broken phase, an energy gap of order $\sim M_f$ was obtained between the branches that have a hyperbolic form. This gap appears as a consequence of the electroweak contributions to the dispersion relations.

The T dependence of the thermal effective masses for the top quark and for the electron neutrino was studied numerically. The results for the massive top quark suggest that two branches become unphysical in the broken phase for $T < 120$ GeV.

We have studied the gauge dependence of the dispersion relations for the massless and massive quark cases in QCD by confronting computations in the Feynman and the Landau gauges. We have found for both cases that the dispersion relations in the Landau gauge are equal to those obtained at leading order in the Feynman gauge.

The fermion dispersion relations in the MSM include leading and sub-leading

contributions. For the unbroken phase, in a similar way as the massless QCD case, the branches in the Landau gauge are superimposed on the Feynman gauge branches at leading order. Consequently, the fermion dispersion relations are gauge invariant at leading order. The consideration of the non-leading terms in the fermion self-energy introduces a small sub-leading gauge dependence in the dispersion relations. General considerations indicate that the sub-leading contribution to the thermal effective masses, in a general gauge, is of order $\sim g_s^3 T$ for quarks and $\sim g^3 T$ for charged leptons and neutrinos. Particularly, the sub-leading contribution in the Feynman gauge is $\delta M^u_{L,R} = \rho M^{u(Lead)}_{L,R}$ for the quark case, where $M^{u(Lead)}_{L,R}$ is the thermal effective mass at leading order in the unbroken phase (see Eqs. (5. 25)) and $\rho \simeq 0.023$. The sub-leading contribution induces a gauge dependence in our numerical computations of nearly 2%.

The fermion dispersion relations in the broken phase are gauge invariant at leading order in temperature and in fermion mass. The small sub-leading contribution to the dispersion relation is gauge dependent. On general grounds, the sub-leading contribution to the thermal effective masses, in a general gauge, is of order $\sim g_s^3[T - M_q]$ for quarks, and of order $\sim g^3[T - M_e]$ for charged leptons and neutrinos. The sub-leading contribution in the Feynman gauge is $\delta M^b_{L,R}(M_q) = \rho M^{b(Lead)}_{L,R}\left[1 - \frac{M_q}{2T}\right] + \sigma \frac{M_q^2}{4T}$, where $M^{b(Lead)}_{L,R}$ are the thermal effective masses at leading order in the broken phase (see Eq. (5. 29)), and the gauge parameters $\rho \simeq 0.023$ and $\sigma \simeq 0.14$. The gauge dependence induced in our numerical computations is about 2% for the light quark case.

The gauge dependence induced in the shift of the thermal effective masses between the two phases is smaller than the one mentioned above. The difference between the gauge dependent contributions to the thermal effective masses in a general gauge is of order $\sim g_s^3 M_q$ for quarks and of order $\sim g^3 M_e$ for charged leptons and neutrinos. This difference for light quarks in the Feynman gauge is: $\delta M^u_{L,R} - \delta M^b_{L,R} \simeq \rho M^{b(Lead)}_{L,R} \frac{M_q}{2T} - \sigma \frac{M_q^2}{4T}$. In our numerical computations is true that $\delta M^u_L - \delta M^b_L << M^u_L - M^b_L$, showing that the gauge dependence in the shift is very small.

Acknowledgements

We are indebted to Belén Gavela and Olivier Pène for important suggestions and comments about the elaboration of the present work. We also thank Alvaro de Rújula, Pilar Hernández, Jean Orloff, Juan Carlos Pinto, Nuria Rius and Miguel Angel Vázquez-Mozo for many helpful conversations. C. Quimbay would like to thank COLCIENCIAS (Colombia) for financial support. S. Vargas-Castrillón would like to thank Consejería de Educación y Cultura de la Comunidad Autónoma de Madrid for financial support.

Appendices

A Calculation of Z-tadpole diagram

The generic Z-tadpole diagram in Fig. 1 is given by:

$$\Sigma_{tad}(K) = -i\frac{g^2}{C_W^2}\gamma_\mu \Pi_E D_Z^{\mu\nu}(0) \int \frac{d^4p}{(2\pi)^4} Tr[\gamma_\nu \Pi_I S(p)], \tag{A. 1}$$

where $S(p)$ is the fermionic finite temperature propagator (2. 1), $D_Z^{\mu\nu}(0)$ is the propagator of the Z boson at momentum transfer equal to zero:

$$D_Z^{\mu\nu}(0) = \frac{g^{\mu\nu}}{M_Z^2}, \tag{A. 2}$$

and $\Pi_X = (T_X^3 - Q_X S_W^2)L - Q_X S_W^2 R$, are the chiral operators of the tadpole vertices, with $X = E, I$. Here, E and I refers to external and internal fermion respectively. The expression (A. 1) has the same form as that shown by Nötzold and Raffel in [26] for the particular case of neutrino propagation.

Taking over the expressions of the propagators (2. 1) and (A. 2) in (A. 1) and only considering the real part contribution $\mathrm{Re}\,\Sigma'_{tad}(K)$ of the finite temperature contribution $\Sigma'_{tad}(K)$, we obtain:

$$\mathrm{Re}\,\Sigma'_{tad}(K) = \frac{g^2}{C_W^2}\frac{\Pi_E \Omega_I}{M_Z^2} \int \frac{d^4p}{(2\pi)^3} \not{p}\delta(p^2 - M_i^2) n_f(p), \tag{A. 3}$$

where $n(f)$ is the Fermi-Dirac distribution function given by (2. 6) and $\Omega_I = (T_I^3 - Q_I S_W^2)/2$. We follow the same procedure as the one used for the evaluation of the generic diagrams of Fig. 2. If we multiply (A. 3) by either $\not{K}$ or $\not{u}$, and then take the trace of the product, we obtain:

$$\frac{1}{4}Tr(\not{K}\mathrm{Re}\,\Sigma'_{tad}) = \frac{g^2}{C_W^2}\frac{\Pi_E \Omega_I}{M_Z^2}\ \frac{dp_0 d^3p}{(2\pi)^3}(\omega p_0 - \vec{k}\cdot\vec{p})\delta(p_0^2 - |\vec{p}|^2 - M_I^2) n_f(p), \tag{A. 4}$$

$$\frac{1}{4}Tr(\not{u}\,\mathrm{Re}\,\Sigma'_{tad}) = \frac{g^2}{C_W^2}\frac{\Omega_i \Pi_I}{M_Z^2} \int \frac{dp_0 d^3p}{(2\pi)^3} p_0 \delta(p_0^2 - |\vec{p}|^2 - M_I^2) n_f(p). \tag{A. 5}$$

The argument of the delta-Dirac functions of the expressions (A. 4) and (A. 5) have the zeros when $p_0 = \pm(|\vec{p}|^2 + M_I^2)^{1/2} = \epsilon_I$. When we integrate over p_0, we obtain the positive and the negative contributions of ϵ_I. Immediately, one can see that (A. 5) is zero and the integral (A. 4) is seen to be zero after the angular integration. It is direct to prove that if we take the trace of (A. 3), the result vanishes. As a consequence, the contribution of the Z-tadpole diagram to the real part of the fermionic thermal self-energy is zero. This result differs from that given in [25], where the tadpole diagram contributes to the real part of the neutrino thermal self-energy. This contribution exists because the Fermi-Dirac distribution function used there was defined without the absolute value that we used in (3. 6).

B Real part of the fermion self-energy in the Landau gauge

The thermal propagator in the Landau gauge for massless gauge $D^{\pounds}_{\mu\nu}(p)$ and massless scalar $D^{\pounds}(p)$ bosons are:

$$D^{\pounds}_{\mu\nu}(p) = \left[-g_{\mu\nu} + \frac{p_\mu p_\nu}{p^2}\right]\left[\frac{1}{p^2+i\epsilon} - i\Gamma_b(p)\right], \tag{B. 1}$$

$$D^{\pounds}(p) = \frac{1}{p^2+i\epsilon} - i\Gamma_b(p), \tag{B. 2}$$

with $\Gamma_b(p)$ defined by (3. 5). The contribution to the self-energy from the generic gauge boson one-loop diagram of Fig. 2a is:

$$\Sigma^{\pounds}(K) = ig^2 C_c \int \frac{d^4p}{(2\pi)^4} D^{\pounds}_{\mu\nu}(p)\gamma^\mu S(p+K)\gamma^\nu, \tag{B. 3}$$

where $S(p)$ is given by (3. 1). Inserting the expressions (3. 1) and (B. 1) into (B. 3) and keeping only the real part $\mathrm{Re}\,\Sigma'^{\pounds}(K)$ of the finite temperature contribution $\Sigma'^{\pounds}(K)$ to the self-energy, it is possible to write:

$$\mathrm{Re}\,\Sigma'^{\pounds}(K) = \mathrm{Re}\,\Sigma'(K) + \mathrm{Re}\,\delta\Sigma'(K), \tag{B. 4}$$

where $\mathrm{Re}\,\Sigma'(K)$ is the real part of the finite temperature contribution to the self-energy in the Feynman gauge (3. 8) and $\mathrm{Re}\,\delta\Sigma'(K)$ is given by:

$$\mathrm{Re}\,\delta\Sigma'_0 = g^2 C_c \int \frac{d^4p}{(2\pi)^4} \not{p}(\not{p}+\not{K}+M_1)\not{p}\left[\frac{\Gamma_b(p)}{p^2[(p+K)^2-M_1^2]} - \frac{\Gamma_f(p+K)}{p^4}\right], \tag{B. 5}$$

where the denominators are defined by their principal value. We note that there is a principal-value singularity $1/p^2$ in the longitudinal boson propagator. Its product with $\delta(p^2)$ is defined by $-\delta(p^2)/p^2 \to \delta'(p^2)$, where the prime denotes the derivative with respect to p_0^2 [3]. Using this definition and following a procedure similar to the preceding case, the traces $\frac{1}{4}Tr(\not{K}\mathrm{Re}\,\delta\Sigma'_0)$ and $\frac{1}{4}Tr(\not{u}\,\mathrm{Re}\,\delta\Sigma'_0)$ are calculated. With similar expressions to (3. 15)-(3. 17), the following relations are obtained:

$$a_0^\delta(\omega,k) = g^2 C_c A_0^\delta(M_1,0), \tag{B. 6}$$

$$b_0^\delta(\omega,k) = g^2 C_c B_0^\delta(M_1,0), \tag{B. 7}$$

$$c_0^\delta(\omega,k) = \frac{g^2 C_c}{2}\frac{M_1}{M_I} C(M_1,0), \tag{B. 8}$$

where:

$$A_0^\delta(M_1,0)=\int_0^\infty \frac{dp}{4\pi^2}\frac{1}{k^2}\left(\left[\frac{\omega^2-k^2-M_1^2}{2p}+\frac{\omega^2-k^2-M_1^2}{2T}e^{P/T}n_B(p)\left(1+2\frac{\omega}{k}L_2^-(p)\right)\right.\right.$$
$$-\frac{1}{2}\left(\omega R^-(p)+pR^+(p)\right)-\omega p\left(\omega T^+(p)+pT^-(p)\right)$$
$$-\left(\frac{\omega^2-k^2-M_1^2}{8k}-\frac{(\omega^2-k^2-M_1^2)^2}{16kp}\left[\frac{1}{p}+\frac{1}{T}e^{p/T}n_B(p)\right]\right)L_2^+(p)\Bigg]n_B(p)$$
$$\left.+\frac{p}{\epsilon_1}\left[\frac{\omega^2+k^2}{8k}L_1^+(p)-\frac{1}{2}pS^+(p)+\omega\epsilon_1 pU^-(p)+\omega^2 pV^+(p)\right]n_F(\epsilon_1)\right). \quad \text{(B. 9)}$$

$$B_0^\delta(M_1,0)=-\int_0^\infty \frac{dp}{4\pi^2}\frac{1}{k^2}\left(\left[\frac{\omega(\omega^2-k^2-M_1^2)}{2p}\right.\right.$$
$$+\frac{\omega^2-k^2-M_1^2}{2T}e^{P/T}n_B(p)\left(\omega+2\frac{(\omega^2-k^2)}{k}L_2^-(p)\right)$$
$$-\frac{1}{2}\omega\left(\omega R^-(p)+pR^+(p)\right)-(\omega^2-k^2)p\left(\omega T^+(p)+pT^-(p)\right)$$
$$-\left(\frac{\omega(\omega^2-k^2-M_1^2)}{8k}-\frac{\omega(\omega^2-k^2-M_1^2)^2}{16kp}\left[\frac{1}{p}+\frac{1}{T}e^{p/T}n_B(p)\right]\right)L_2^+(p)\Bigg]n_B(p)$$
$$\left.+\frac{p}{\epsilon_1}\left[\frac{\omega(\omega^2-k^2)}{8k}L_1^+(p)+\frac{\omega}{2}pS^+(p)+\epsilon_1(\omega^2-k^2)pU^-(p)+\right]n_F(\epsilon_1)\right). \quad \text{(B. 10)}$$

$C(M_1,0)$ is given by (3. 23) with $M_2=0$. The functions defined in (B. 9) and (B. 10) are:

$$R^\pm(p)=\frac{(\omega^2-k^2-M_1^2)^2}{(\omega^2-k^2-M_1^2+2\omega p)^2-4k^2p^2}\pm\frac{(\omega^2-k^2-M_1^2)^2}{(\omega^2-k^2-M_1^2-2\omega p)^2-4k^2p^2}, \quad \text{(B. 11)}$$

$$S^\pm(p)=\frac{(\omega^2-k^2)(\omega^2-k^2+M_1^2)}{(\omega^2-k^2+M_1^2+2\omega\epsilon_1)^2-4k^2p^2}\pm\frac{(\omega^2-k^2)(\omega^2-k^2+M_1^2)}{(\omega^2-k^2+M_1^2-2\omega\epsilon_1)^2-4k^2p^2}, \quad \text{(B. 12)}$$

$$T^\pm(p)=\frac{(\omega^2-k^2-M_1^2)}{(\omega^2-k^2+M_1^2+2\omega\epsilon_1)^2-4k^2p^2}\pm\frac{(\omega^2-k^2-M_1^2)}{(\omega^2-k^2+M_1^2-2\omega\epsilon_1)^2-4k^2p^2}, \quad \text{(B. 13)}$$

$$U^\pm(p)=\frac{(\omega^2-k^2)}{(\omega^2-k^2+M_1^2+2\omega\epsilon_1)^2-4k^2p^2}\pm\frac{(\omega^2-k^2)}{(\omega^2-k^2+M_1^2-2\omega\epsilon_1)^2-4k^2p^2}, \quad \text{(B. 14)}$$

$$V^\pm(p)=\frac{(\omega^2-k^2+M_1^2)}{(\omega^2-k^2+M_1^2+2\omega\epsilon_1)^2-4k^2p^2}\pm\frac{(\omega^2-k^2+M_1^2)}{(\omega^2-k^2+M_1^2-2\omega\epsilon_1)^2-4k^2p^2}, \quad \text{(B. 15)}$$

and the functions $L_1^\pm$ and $L_2^\pm$ given by (3. 13)-(3. 14) with $M_2=0$.

The Lorentz-invariant functions in the Landau gauge are given by

$$a^{\pounds}(\omega,k) = g^2 C_c A^{\pounds}(M_1,0), \tag{B. 16}$$

$$b^{\pounds}(\omega,k) = g^2 C_c B^{\pounds}(M_1,0), \tag{B. 17}$$

$$c^{\pounds}(\omega,k) = \frac{5}{2} g^2 C_c \frac{M_1}{M_I} C(M_1,0), \tag{B. 18}$$

where

$$A^{\pounds}(M_1,0) = A(M_1,0) + A_0^{\delta}(M_1,0), \tag{B. 19}$$

$$B^{\pounds}(M_1,0) = B(M_1,0) + B_0^{\delta}(M_1,0), \tag{B. 20}$$

with $A(M_1,0)$, $B(M_1,0)$ and $C(M_1,0)$ given by (3. 21)-(3. 23), with $M_2 = 0$. $A_0^{\delta}(M_1,0)$ and $B^{\pounds}(M_1,0)$ are given by (B. 9) and (B. 10).

C Lorentz-invariant functions in the Landau gauge

The chiral projections of the Lorentz-invariant functions for the quarks in the unbroken phase are given by:

$$a^{\pounds}_{\substack{L\\R}}(\omega,k)_{IF} = \bar{f}^1_{\substack{L\\R}} A(0,0) + \bar{f}^2_{\substack{L\\R}} A_0^{\delta}(0,0), \tag{C. 1}$$

$$b^{\pounds}_{\substack{L\\R}}(\omega,k)_{IF} = \bar{f}^1_{\substack{L\\R}} B(0,0) + \bar{f}^2_{\substack{L\\R}} B_0^{\delta}(0,0), \tag{C. 2}$$

where the integrals $A(0,0)$ and $B(0,0)$ are given by (3. 21) and (3. 22), with $M_1 = M_2 = 0$. The integrals $A_0^{\delta}(0,0)$ and $B_0^{\delta}(0,0)$ are defined by (B. 9) and (B. 10), with $M_1 = 0$. The coefficients are:

$$\bar{f}^1_L = 8\left\{\left(\frac{2\pi\alpha_S}{3} + \frac{3\pi\alpha_W}{8}\left[1 + \frac{\tan^2\theta_W}{27} + \frac{1}{3}\lambda_I^2\right]\right)\delta_{IF} + \frac{\pi\alpha_W}{8} K^+_{Ii}\lambda_i^2 K_{iF}\right\}, \tag{C. 3}$$

$$\bar{f}^2_L = 8\left\{\frac{2\pi\alpha_S}{3} + \frac{3\pi\alpha_W}{8}\left[1 + \frac{\tan^2\theta_W}{27}\right]\right\}\delta_{IF}, \tag{C. 4}$$

$$\bar{f}^1_R = 8\left\{\frac{2\pi\alpha_S}{3} + \frac{\pi\alpha_W}{2}\left[Q_I^2\tan^2\theta_W + \frac{1}{2}\lambda_I^2\right]\right\}\delta_{IF}, \tag{C. 5}$$

$$\bar{f}^2_R = 8\left\{\frac{2\pi\alpha_S}{3} + \frac{\pi\alpha_W}{2}\left[Q_I^2\tan^2\theta_W\right]\right\}\delta_{IF}. \tag{C. 6}$$

The chiral projections of the Lorentz-invariant functions for charged leptons are:

$$a^{\pounds}_{\substack{L\\R}}(\omega,k) = \bar{d}^1_{\substack{L\\R}} A(0,0) + \bar{d}^2_{\substack{L\\R}} A_0^{\delta}(0,0), \tag{C. 7}$$

$$b^{\pounds}_{\substack{L\\R}}(\omega,k) = \bar{d}^1_{\substack{L\\R}} B(0,0) + \bar{d}^2_{\substack{L\\R}} B_0^{\delta}(0,0), \tag{C. 8}$$

where the integrals $A(0,0)$ and $B(0,0)$ are given by (3. 21) and (3. 22), with $M_1 = M_2 = 0$. The integrals $A_0^\delta(0,0)$ and $B_0^\delta(0,0)$ are defined by (B. 9) and (B. 10), with $M_1 = 0$. The coefficients are:

$$\bar{d}_L^1 = \pi\alpha_W \left[2 + \frac{1}{c_w^2} + \lambda_e^2\right], \tag{C. 9}$$

$$\bar{d}_L^2 = \pi\alpha_W \left[2 + \frac{1}{c_w^2}\right], \tag{C. 10}$$

$$\bar{d}_R^1 = 4\pi\alpha_W \left[\tan^2\theta_W + \frac{\lambda_e^2}{2}\right], \tag{C. 11}$$

$$\bar{d}_R^2 = 4\pi\alpha_W \left[\tan^2\theta_W\right]. \tag{C. 12}$$

The chiral projections of the Lorentz-invariant functions for neutrinos are:

$$a_L^{\not{\epsilon}}(\omega,k) = \bar{v}^1 A(0,0) + \bar{v}^2 A_0^\delta(0,0), \tag{C. 13}$$

$$b_L^{\not{\epsilon}}(\omega,k) = \bar{v}^1 B(0,0) + \bar{v}^2 B_0^\delta(0,0), \tag{C. 14}$$

where the integrals $A(0,0)$ and $B(0,0)$ are given by (3. 21) and (3.22), with $M_1 = M_2 = 0$. The integrals $A_0^\delta(0,0)$ and $B_0^\delta(0,0)$ are defined by (B. 9) and (B. 10), with $M_1 = 0$. The coefficients are:

$$\bar{v}^1 = \pi\alpha_W \left[2 + \frac{1}{c_w^2} + \lambda_e^2\right], \tag{C. 15}$$

$$\bar{v}^2 = \pi\alpha_W \left[2 + \frac{1}{c_w^2}\right]. \tag{C. 16}$$

References

[1] G. R. Farrar and M. E. Shaposhnikov, Phys. Rev. **D50**, 774 (1994).

[2] M. B. Gavela, P. Hernández, J. Orloff, O. Pène and C. Quimbay, Nucl. Phys. **B430**, 382 (1994).

[3] H. A. Weldon, Phys. Rev. **D26**, 2789 (1982).

[4] H. A. Weldon, Physica **A158**, 169 (1989)

[5] H. A. Weldon, Phys. Rev. **D40**, 2410 (1989).

[6] R. Pisarski, Nucl. Phys. **A498**, 423c (1989).

[7] J. P. Blaizot and J. Y. Ollitrault, Phys. Rev. **D48**, 1390 (1993).

[8] E. Petitgirard, Z. Phys. **C54**, 673 (1992).

[9] D. A. Kirzhnits, JETP Lett. **15**, 745 (1972); D. A. Kirzhnits and A. D. Linde, Phys. Lett. **42B**, 471 (1972); A. D. Linde, JETP Lett. **19**, 320 (1974).

[10] H. A. Weldon, Phys. Rev. **D28**, 2007 (1983); R. Kobes and G. Semenoff, Nucl. Phys. **B260**, 714 (1985) and **B272**, 329 (1986); J. C. D'Olivo and J. F. Nieves, Damping rate of a fermion in a medium, University of Puerto Rico, Department of Physics, July 1993.

[11] E. Braaten and R. D. Pisarski, Phys. Rev. **D46**, 1829 (1992); R. Kobes, G. Kunstatter and K. Mak, Phys. Rev. **D45**, 4632 (1992).

[12] P. Huet and E. Sather, Phys. Rev. **D51**, 379 (1995).

[13] Z. Fodor, J. Hein, K. Jaster and I. Montvay, Simulating the electroweak phase transition in the SU(2) Higgs model, DESY 94-159, September 1994.

[14] S. L. Dolan and R. Jackiw, Phys. Rev. **D9**, 3320 (1974); A. J. Niemi and G. W. Semenoff, Ann. Phys. (N.Y.) **152**, 105 (1984); N. P. Landsman and Ch. G. van Weert, Phys. Rep. **145**, 141 (1987).

[15] D. Seibert, The high-frequency finite-temperature quark dispersion relation, CERN-TH. 7034/93.

[16] T. Altherr and P. Aurenche, Phys. Rev. **D40**, 4171 (1989).

[17] V. V. Lebedev and A. V. Smilga, Ann. Phys. (N.Y.) **202**, 229 (1990).

[18] V. V. Klimov, Sov. J. Nucl. Phys. **33**, 934 (1981); Sov. Phys. JETP **55**, 199 (1982).

[19] A. Bechler, Ann. Phys. (N.Y.) **135**, 19 (1981); G. Peressutti and B.-S. Skagerstam, Phys. Lett. **B110**, 406 (1982); J. F. Donoghue, B. R. Hilstein and R. W. Robinett, Ann. Phys. (N.Y.) **164**, 233 (1985).

[20] E. J. Levinson and D. H. Boal, Phys. Rev. **D31**, 3280 (1985).

[21] M.-C. Chu, S. Huang and J. A. Lee, Phys. Rev. **D48**, 3901 (1993).

[22] G. Baym, J. P. Blaizot and J. Polonyi, Nucl. Phys. **B230**, 4043 (1992).

[23] A. J. Niemi and G. W. Semenoff, Nucl. Phys. **B230**, 181 (1984); K. Takahashi, Phys. Rev. **D29**, 632 (1984); T. Toimela, Nucl. Phys. **B273**, 719 (1986).

[24] E. Braaten and R. D. Pisarski, Phys. Rev. Lett. **64**, 1338 (1990); Nucl. Phys. **B337**, 569 (1990) and **B339**, 310 (1990); Phys. Rev. **D42**, 2156 (1990); E. Braaten, Ap. J. **392**, 70 (1992).

[25] J. C. D'Olivo, J. F. Nieves and M. Torres, Phys. Rev. **D46**, 1172 (1992).

[26] D. Nötzold and G. Raffelt, Nucl. Phys. **B307**, 924 (1989).

[27] K. Enquist, K. Kainulainen and J. Maalampi, Nucl. Phys. **B349**, 754 (1991).

[28] J. F. Nieves, Phys. Rev. **D40**, 866 (1989).

[29] P. B. Pal and T. N. Pham, Phys. Rev. **D40**, 259 (1989).

[30] A. Erdas, C. W. Kim and J. A. Lee, Phys. Rev. **D48**, 3901 (1993).

[31] A. Erdas, C. W. Kim and J. A. Lee, Generational mass splitting of neutrinos in high temperature $SU(2)_L \otimes U(1)_Y$ gauge theory, JHU-TIPA-940008, INFNCA-TH-94-8.

[32] R. Kobes, G. Kunstatter and R. Rebhan, Nucl. Phys. **B355**, 1 (1991); Phys. Rev. Lett. **64**, 2992 (1990).

[33] J. Frenkel and J.C. Taylor, Nucl. Phys, **B334**, 199 (1990); J.C. Taylor and S.M.H. Wong, Nucl. Phys. **B346**, 115 (1990).

[34] H. Schulz, Nucl. Phys. **B413**, 353 (1994); R. Baier, G. Kunstatter and D. Schiff, Nucl. Phys. **B388**, 287 (1992).

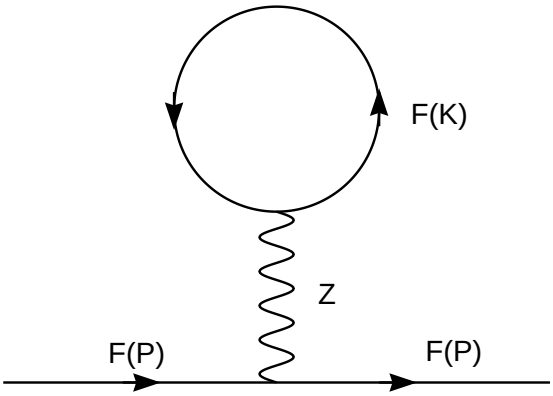

Figure 1: Generic Z-tadpole diagram

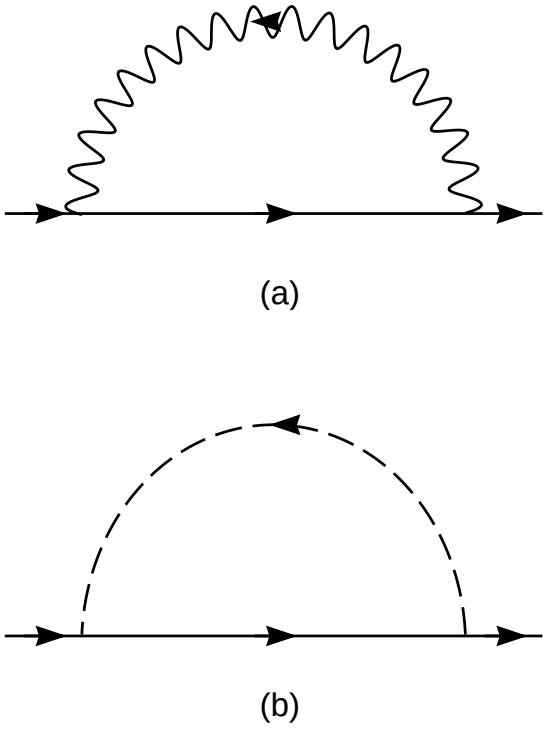

Figure 2: Generic gauge and scalar boson diagrams

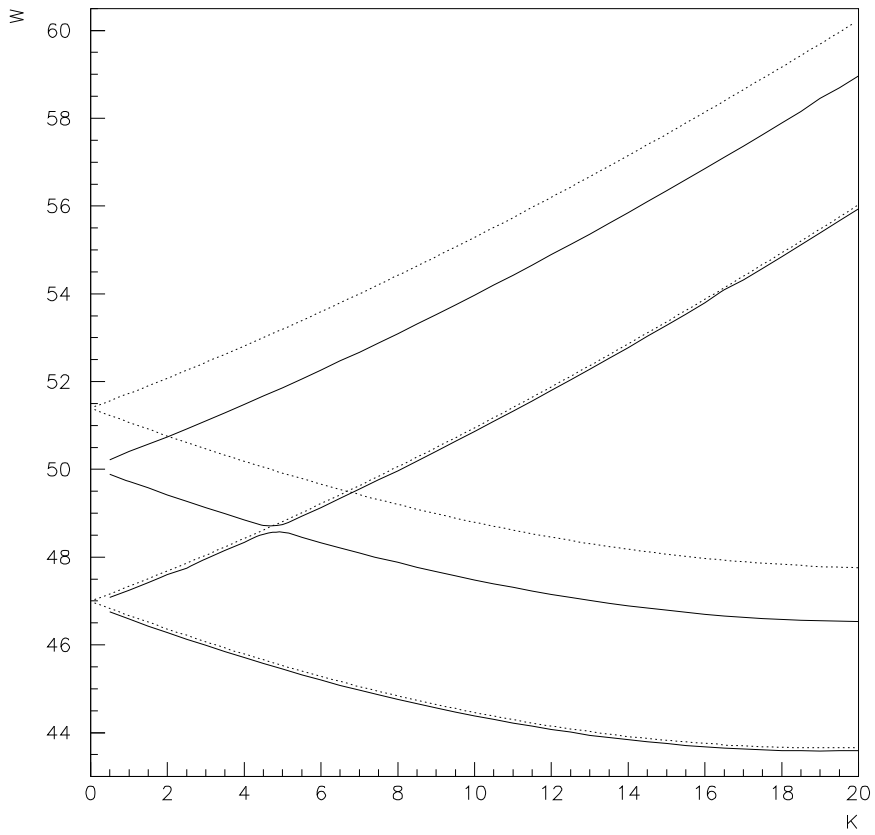

Figure 3: Dispersion relations at $T = 100$ GeV for the s quark in the broken (solid curves) and the unbroken (dotted curves) phases, neglecting quark mixing. The upper (lower) dotted curves correspond to left (right) chirality branches. An energy gap ($\simeq 0.1$ GeV) appears between the minimum and maximum of the hyperbolic branches.

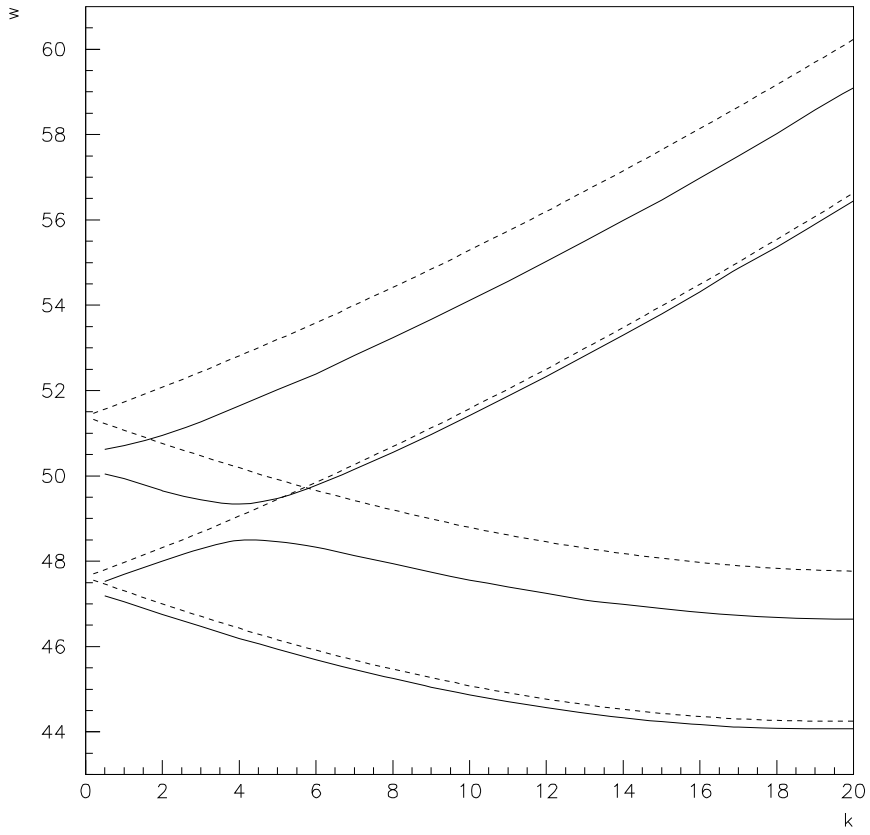

Figure 4: Dispersion relations at $T = 100$ GeV for the c quark in the broken (solid curves) and the unbroken (dashed curves) phases, neglecting quark mixing. The energy gap between the hyperbolic branches is $\simeq 1.0$ GeV. The thermal effective masses for the branches in the broken phase are smaller that those in the unbroken phase.

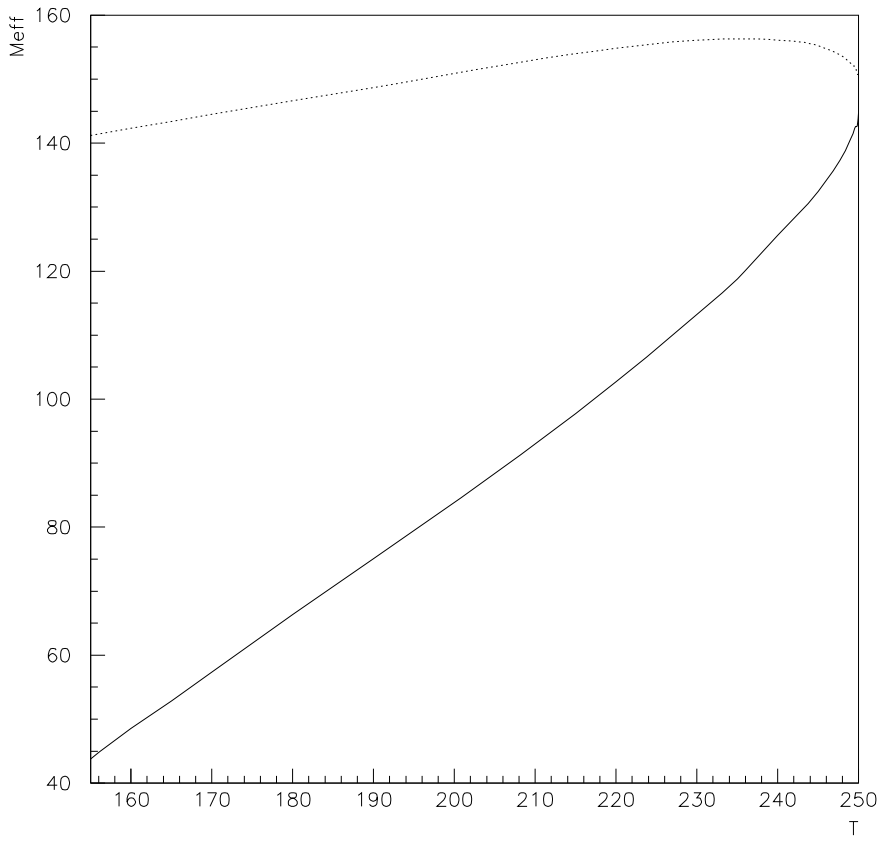

Figure 5: Variation with temperature of the thermal effective masses for the top quark in the broken phase.

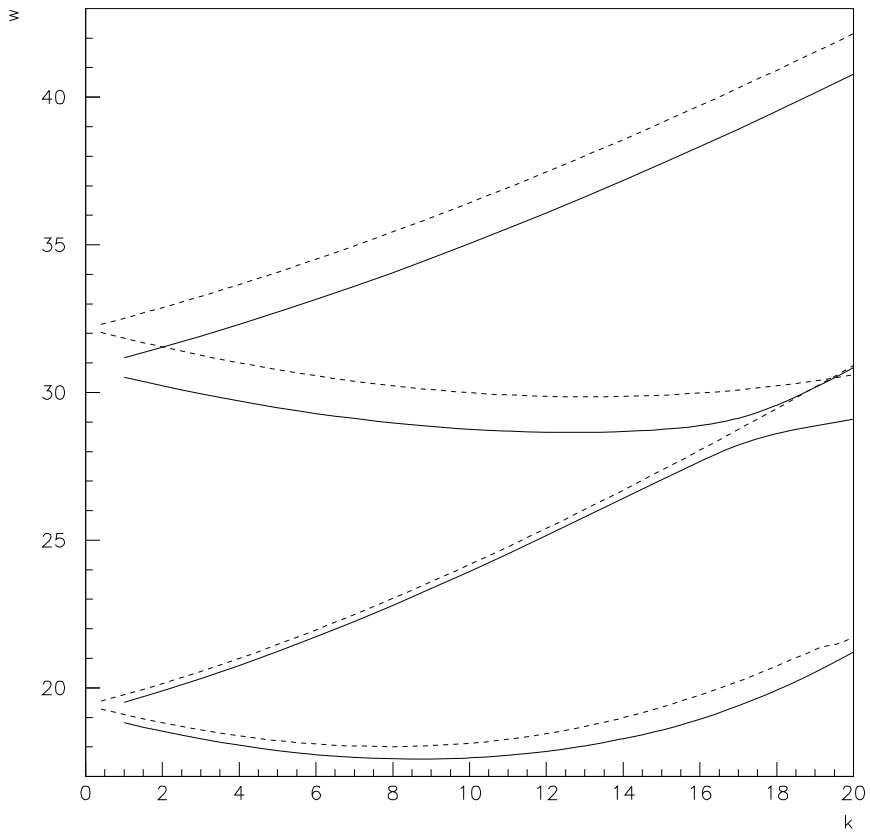

Figure 6: Dispersion relations at $T = 150$ GeV for the τ lepton in the broken (solid curves) and the unbroken (dashed curves).

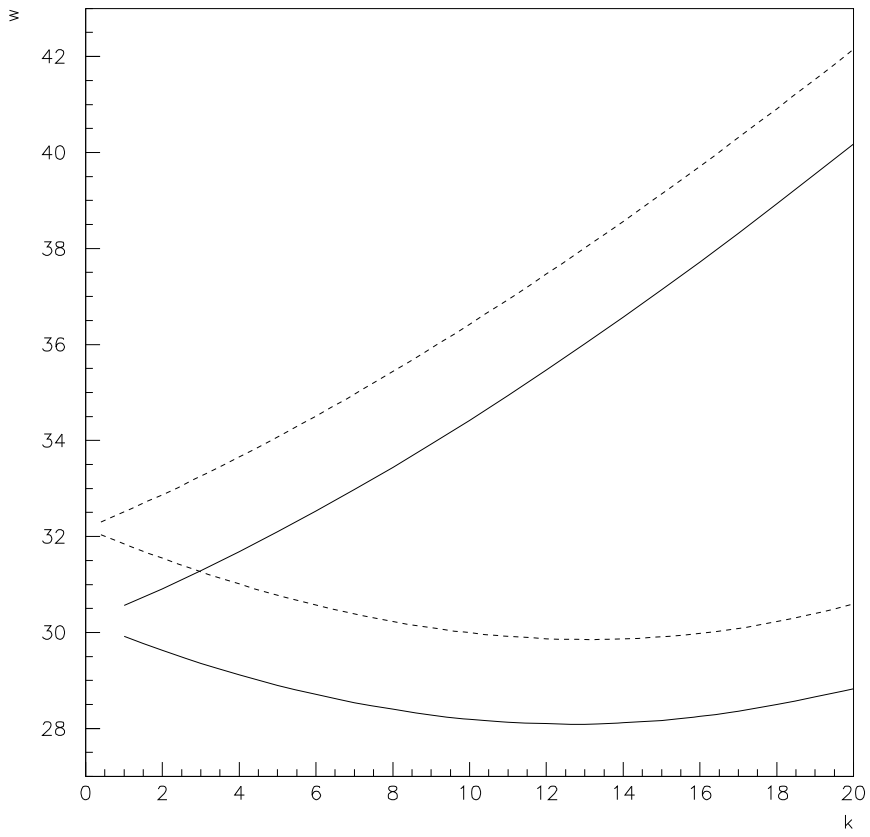

Figure 7: Dispersion relations at $T = 150$ GeV for the electron neutrino in the broken (solid curves) and the unbroken (dashed curves) phases.

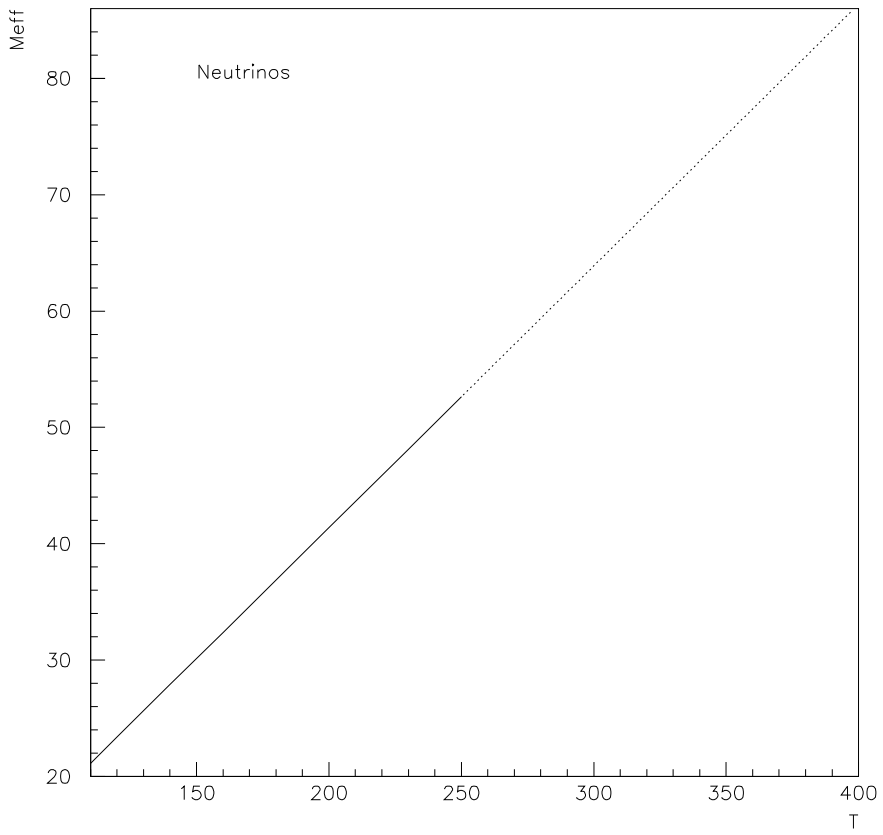

Figure 8: Variation with temperature of the electron-neutrino thermal effective masses for the broken (solid curves) and unbroken (dotted curves) phases

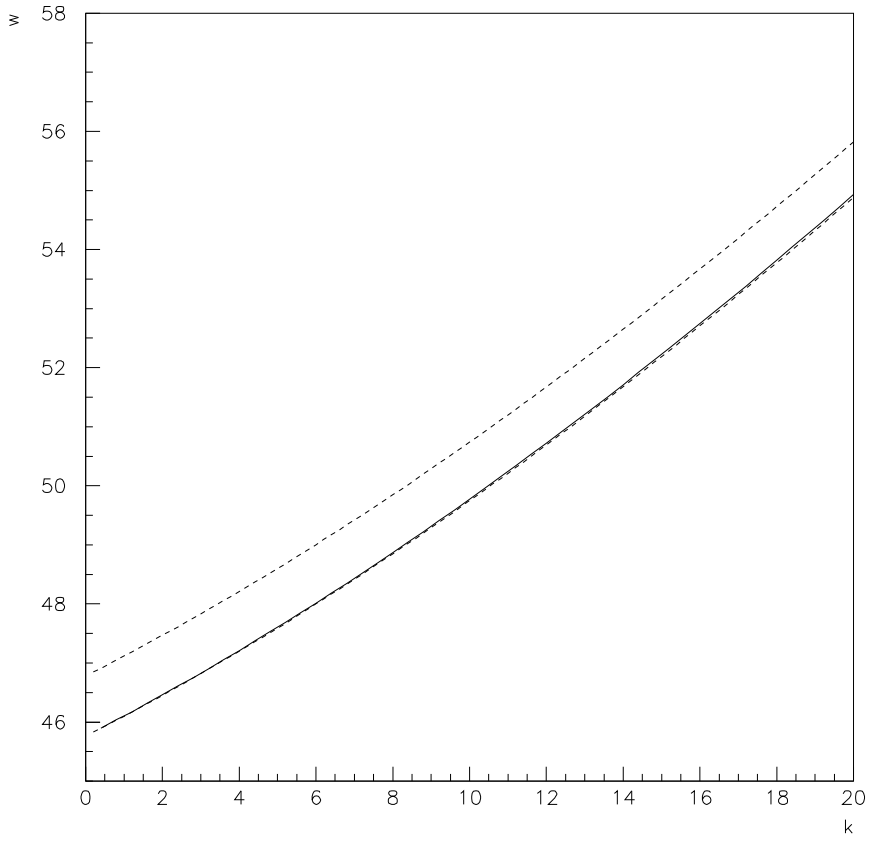

Figure 9: Normal branch for the massless b quark in QCD computed for three different cases at $T = 100$ GeV. The lower dashed curve is computed in the Feynman gauge considering only the leading $\mathcal{O}(T^2)$ contribution to the self-energy (leading curve). The upper dashed curve corresponds to the results in the Feynman gauge considering all the contributions to the self energy (Feynman curve). The solid curve is computed in the Landau gauge also considering all the contributions (Landau curve). The leading and Landau curves are superimposed.

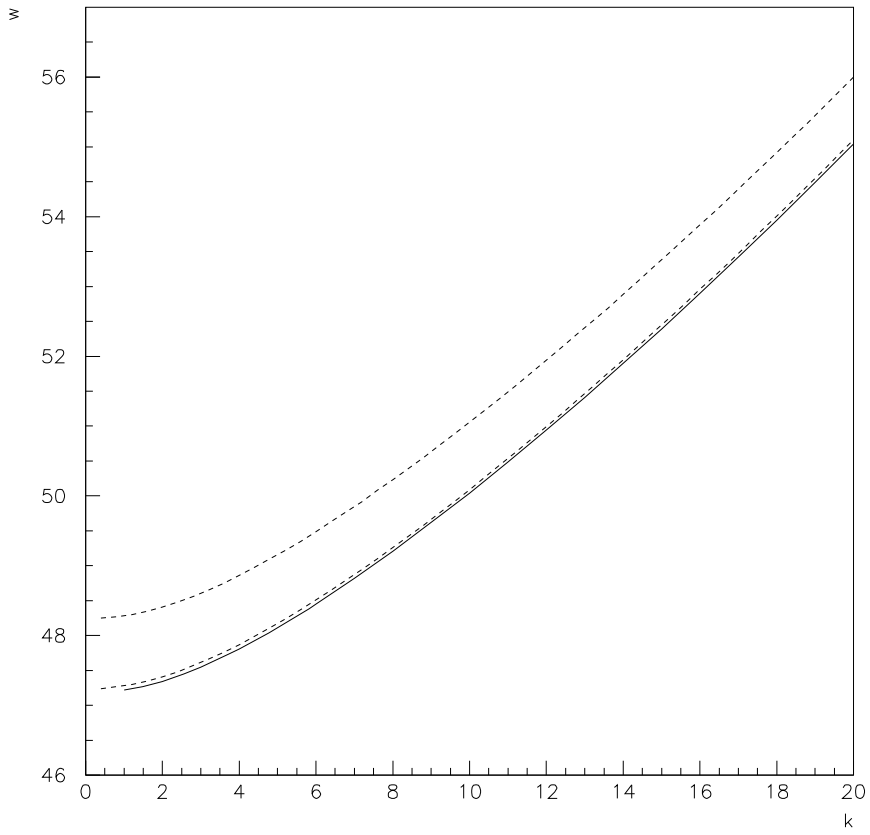

Figure 10: Normal branch for the massive b quark in QCD computed for three different cases at $T = 100$ GeV. The lower dashed curve is computed in the Feynman gauge considering only the leading $\mathcal{O}(T^2)$ contribution to the self-energy (leading curve). The upper dashed curve corresponds to the results in the Feynman gauge considering all the contributions to the self-energy (Feynman curve). The solid curve is computed in the Landau gauge also considering all the contributions (Landau curve). The leading and Landau curves are superimposed.